Groundwater recharge in formerly glaciated terrain: Exploring the relationship between frost dynamics, precipitation, and snowmelt in a Northeastern Minnesota deranged drainage basin

A Thesis

SUBMITTED TO THE FACULTY OF THE UNIVERSITY OF MINNESOTA

BY

Mitchell D. Ihlang

IN PARTIAL FULFILLMENT OF THE REQUIREMENTS FOR THE DEGREE OF MASTER OF SCIENCE

Dr. John B. Swenson

Dr. Salli F. Dymond

August 2021

ACKNOWLEDGEMENTS

I would like to thank my research advisors, Dr. John Swenson and Dr. Salli Dymond, for their unending support throughout this project. This project was possible through their expertise, patience, and genuine passion for science. They served as mentors, field hands, troubleshooters, counselors, financers, and friends throughout this process. This project would also not have been possible without the help of Scott Norr, who served as an incredible resource for all the electrical engineering questions that arose from my sensors. What I appreciated the most about Scott was his eagerness to help, whether it be with wiring, coding, or design.

I would also like to thank the other members of Dr. Dymond's WaTER Lab, the other WRS and GS graduate students in my cohort, and the entire Department of Earth and Environmental Sciences faculty. More specifically, I would like to thank Dr. Howard Mooers and Dr. Karen Gran for allowing me to borrow equipment and resources throughout this project. My thesis would not have been possible without the use of Howard's drill rig or Karen's flow meter. My thesis also would not have been possible without Julie Agnich, who analyzed the several hundred isotope samples necessary for my project in her lab at the Large Lakes Observatory. I would also like to specifically thank Peter Bouchard, Sam Nesheim, and Erin Bergen for assisting me in my field work. Their time and energy is greatly appreciated.

Lastly, I would like to thank my family for always supporting me through whatever I do in life. I am incredibly proud to be the first member of my family to earn a graduate degree and it would not have been possible without the encouragement and support from my parents, my brother and sister-in-law, and my entire extended family.

TABLE OF CONTENTS

LIST OF FIGURES

LIST OF TABLES

Chapter 1: Introduction

In Minnesota, 75% of all drinking water and 90% of all irrigation is sourced from groundwater (Smith & Westenbroek, 2015). Additionally, as climate warms, changes in both groundwater quality and quantity are expected. A thorough understanding of sustainable groundwater management has thus become increasingly relevant for the region (Henry, 2008; Okkonen et al., 2009; Okkonen & Klöve, 2011). Sustainable management of groundwater resources is dependent on accurate estimations of groundwater recharge, which is often one of the hardest components of the water cycle to measure (de Vries & Simmers, 2002; Delin et al., 2007). Estimating and understanding groundwater recharge is especially difficult in formerly glaciated regions, such as Minnesota, where irregular drainage networks and seasonally frozen ground can cause recharge patterns to vary spatially and temporally (Keller et al., 1988; Van der Kamp & Hayashi, 1998; Jones & Tomasek, 2015; Pam et al., 2020).

Groundwater recharge is thought to occur via three mechanisms: direct groundwater recharge, indirect groundwater recharge, and localized groundwater recharge (de Vries & Simmers, 2002). *Direct groundwater recharge* (also referred to as "diffuse areal recharge") occurs when meteoric water directly infiltrates the soil and percolates down to the water table (Figure 1.1). *Indirect groundwater recharge* results from groundwater-surface water interactions near streams in which the local water table is at a lower elevation than the hydraulic head in the stream (i.e., a "losing" stream) (Figure 1.1; Figure 1.2). Stream water thus recharges the groundwater in this scenario. Lastly, *localized recharge* (more commonly referred to as "depression-focused recharge") occurs in lower-permeability soils where direct infiltration is limited and topographical depressions route most rainfall and snowmelt. If enough water ponds in the depression to exceed the soil moisture storage capacity, this water can recharge the shallow

groundwater system surrounding the depression (Lissey, 1971; Van der Kamp & Hayashi, 1998; Berthold & Hayashi, 2004).

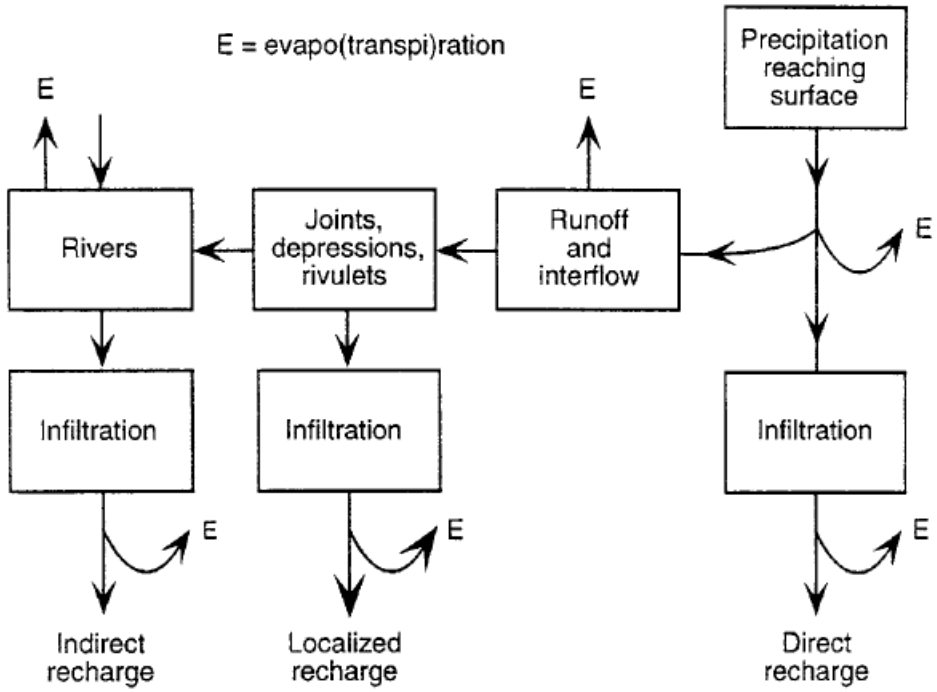

Figure 1.1: Flow diagram of different runoff mechanisms. From Lerner, 1997.

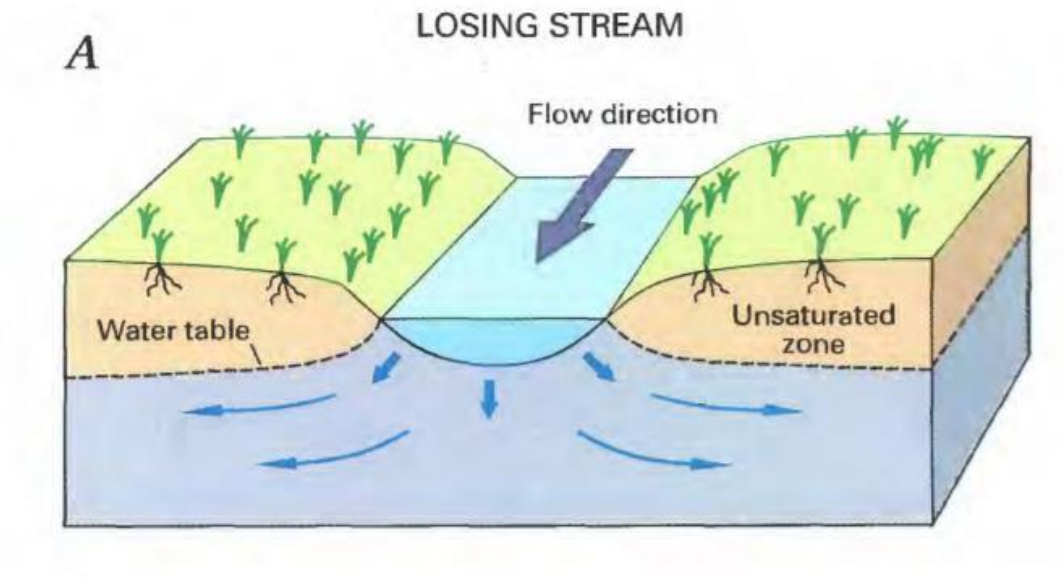

Figure 1.2: Schematic of indirect groundwater recharge occurring underneath a losing stream. From Winter et al., 1998.

In formerly-glaciated regions such as Northeastern Minnesota, the mechanisms of recharge are largely controlled by relatively young, poorly-developed surface drainage (Fortin et al., 1991; Jones & Tomasek, 2015). The advance and retreat of glaciers over a landscape can completely reshape the underlying terrain, erasing previously developed drainage networks (Zernitz, 1932). The result is an irregular drainage network with no coherent pattern in its distribution of surface water bodies, referred to as "deranged" or "glacially disturbed" (Zernitz, 1932; Fortin et al., 1991; Duk-Rodkin & Hughes, 1994). The deposition of clay- and silt-rich glacial tills also restricts infiltration and percolation in the region, thereby limiting direct groundwater recharge and promoting depression-focused recharge (Keller et al., 1988; Fortin et al., 1991; Hayashi et al., 2016; Mohammed et al., 2019; Pavlovskii et al., 2019). Despite the low hydraulic conductivity of tills, bulk permeability can be relatively high near the soil surface due to preferential flow features formed from oxidation and weathering (Fritz et al., 1976; Desaulniers et al., 1981; D'Astous et al., 1989; Hendry et al., 2004; Van der Kamp & Hayashi, 2009). As a result, the surficial reaches of a till unit may have relatively active groundwater flow systems, while recharge through deeper tills becomes increasingly limited (Keller et al., 1988; Hayashi et al., 2016).

The relatively active shallow groundwater systems in surficial glacial tills can be vulnerable to the influence of artificial drainage networks (e.g., tile drainage). In Northeastern Minnesota, tile drainage is common and can alter groundwater flow and recharge processes by routing rainfall and meltwater away from depressions, limiting the overall amount of recharge that can occur at a given site. Additionally, tile drainage that was installed prior to 1955 typically used concrete that was susceptible to degradation when exposed to sulfates within subsurface waters (Minnesota Groundwater Association, 2018). As a result, several older drain tiles in Northeastern Minnesota have collapsed, causing an unintended redistribution of surface drainage.

The specific influence of tile drainage on shallow groundwater systems in glacial tills has not been studied extensively (Minnesota Groundwater Association, 2018).

In colder climates such as Northeastern Minnesota, the development of soil frost during cold winters can also limit infiltration and percolation (Kane & Stein, 1983; Johnsson & Lundin, 1991; Pittman et al., 2019). Snowmelt is generally considered the largest single recharge event of the year in colder regions and it often occurs while the ground is still frozen or in the process of thawing (Baker & Spaans, 1997; Pomeroy & Brun, 2001; Hayashi et al., 2003). Several studies have documented groundwater recharge being initiated before the ground is fully thawed, illustrating that infiltration and percolation is still possible through frozen ground (Jansson & Gustafsson, 1987; Thunholm et al., 1989; Johnsson & Lundin, 1991; Daniel & Staricka, 2000; Stahli et al., 2001; Mohammed et al., 2019). This phenomenon occurs under certain conditions relevant to antecedent water contents in the soil, frost depth, the presence of macropores, and the timing and progression of snowmelt (Johnsson & Lundin, 1991; Daniel & Staricka, 2000; Iwata et al., 2011; Pavlovskii et al., 2019; Pittman et al., 2019). In the literature, most attention has been focused on antecedent moisture conditions and macropore networks (Kane & Stein, 1983; Daniel & Staricka, 2000; Weigert & Schmidt, 2005; Watanabe & Kugisaki, 2017; Mohammed et al., 2018; Pittman et al., 2019). While the temporal relationship between frost dynamics, infiltration, and runoff has been studied (Thorne et al., 1998; Hardy et al., 2001; Iwata et al., 2011; Watanabe et al., 2012; Mohammed et al., 2019), the implications of this relationship for groundwater recharge are still poorly-understood (Mohammed et al., 2019).

While the hydrogeology of glacial tills has been studied extensively, little is known about the influence of frost dynamics on the timing of near-surface recharge processes. These recharge processes include infiltration, percolation, and shallow subsurface flow. Additionally, the specific influence of artificial drainage networks on near-surface recharge processes has not been studied. The objectives of this study are as follows:

1) To assess the fate and transport of rainfall and snowmelt within shallow, till-dominated soils in order to examine the timing and pathways of groundwater flow at the hillslope-scale in a formerly glaciated region.
2) To explore the relationship between frost dynamics, precipitation, snowmelt, and infiltration in the context of groundwater recharge to better understand the timing of recharge processes in relation to other hydrological processes.
3) To develop a conceptual model to explain shallow groundwater movement throughout the site following rainfall and snowmelt, focusing on the influence of frost dynamics and tile drainage on the timing, mechanisms, and magnitude of shallow groundwater recharge.

CHAPTER 2: Background/Literature Review

2.1) Spatiotemporal Patterns in Groundwater Recharge

The timing and amount of groundwater recharge in an area depends heavily on the interactions between climate, geology, soils, and vegetation and thus displays significant spatiotemporal variability (de Vries & Simmers, 2002; Nolan et al., 2003; Delin et al., 2007; Dripps & Bradbury, 2009). The effects of spatial variability on groundwater recharge are more pronounced in smaller-scale studies and thus should be accounted for in recharge estimates (Dripps & Bradbury, 2007). In the Midwestern United States, soil texture and land cover tend to have the largest spatial influence on groundwater recharge distribution (Nolan et al., 2003; Dripps & Bradbury, 2009). In these basins, elevation and precipitation are more evenly distributed and thus are thought to have less of an effect on the spatial variability of recharge. However, Delin et al. (2007) found that recharge rates were strongly correlated to mean annual precipitation in Minnesota and that the highest recharge rates in the state were in the Northeast (Figure 2.1), which generally receives more rainfall than the western portions of the state. This contradicts other studies that have reported slow recharge rates (on the order of centimeters per year) through glacial tills, which are common in Northeastern Minnesota (Desaulniers et al., 1989; Hayashi et al., 2016).

Soil texture directly influences infiltration capacity, water holding capacity, and hydraulic conductivity, and thus has a direct influence on the spatial distribution of recharge. Coarser-grained soils have greater infiltration capacity and less storage capacity than finer-grained soils; as a result, recharge is usually inversely proportional to percent clay content (Nolan et al., 2003; Dripps & Bradbury, 2009). Heterogeneity within soils can also cause preferential flow of groundwater movement and affect the resulting groundwater recharge (Hardy et al., 2001; Hendry et al., 2004; Chesnaux et al., 2018). Soil texture also influences water table elevation, with less

permeable soils displaying greater spatial variability in water table elevation (Keller et al., 1988; Pam et al., 2020). Since water table elevation has a direct influence on diffuse recharge, this variability should be accounted for in recharge estimations (Batelaan & Smedt, 2007).

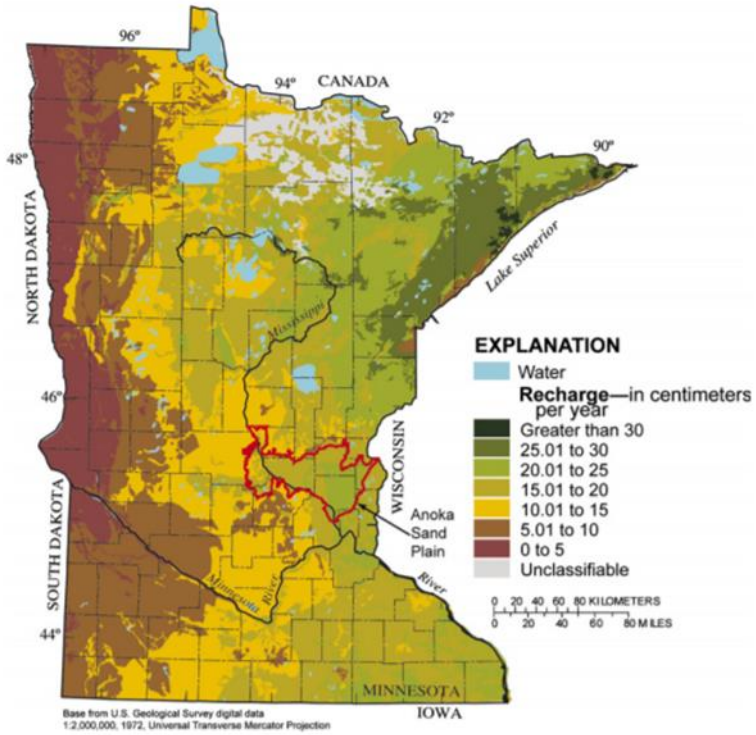

Figure 2.1 Spatial variability in groundwater recharge in Minnesota, estimated using the Regional Regression Method. From Delin et al., 2007.

Diffuse recharge is typically the dominant recharge mechanism in areas with permeable, homogenous vadose zones where water can easily infiltrate and percolate to the water table (de Vries & Simmers, 2002; Chesnaux et al., 2018). In areas with low-permeability glacial tills, most recharge occurs via depression-focused recharge (Keller et al., 1988; Fortin et al., 1991; Berthold & Hayashi, 2003; Mohammed et al., 2019; Pavlovskii et al., 2019). The effects of depression-focused recharge are highly localized to the shallow groundwater systems surrounding the depressions, leading to more spatial variability in recharge distributions (Jones & Tomasek, 2015). However, numerous depressions can be distributed somewhat evenly across a landscape

and can minimize the localized effects of depression-focused recharge (Hayashi et al., 2016). Rerouting of surface runoff via artificial drainage networks (e.g., tile drainage) can thus have a significant effect on the amount and distribution of recharge occurring under lower-permeability sites (Keller et al., 1988; Daniel & Staricka, 2000; Hayashi et al., 2016).

Meanwhile, temporal variability in recharge is largely dependent on the timing and amount of precipitation, and can vary both inter-annually and intra-annually (de Vries & Simmers, 2002; Delin et al., 2007; Dripps & Bradbury, 2009). Intra-annual variability is generally dependent on how different components of the water cycle, such as evapotranspiration, vary throughout the year (de Vries & Simmers, 2002). Seasonality in recharge is also high in formerly glaciated basins across the north central U.S. due to significant seasonal variations in precipitation and large snowfall accumulations (Dripps & Bradbury, 2009). In these regions, spring snowmelt is often the largest recharge event of the year due to the large amount of water available for infiltration and the reduced influence of vegetation (Winograd et al., 1998; Pomeroy & Brun, 2001; Earman et al., 2006). Low vegetative water use also allows for significant recharge events to occur in the fall, which, in some cases, can contribute up to 50% of annual recharge (O'Driscoll et al., 2005; Lee & Kim, 2006; Kim, 2009; Adomako et al., 2010). Recharge in the summer is usually limited to larger rainfall events, while recharge in the winter is thought to be negligible due to the reduced infiltration capacity of frozen soils (O'Driscoll et al., 2005; Dripps & Bradbury, 2009). However, significant recharge events have been reported during the winter in Northern Ireland (McConville et al., 2005) and the Netherlands (Batelaan & Smedt, 2007). The disagreement between different studies highlights the importance of the coupling between spatial and temporal controls on groundwater recharge.

The magnitude of observed recharge events is also related to rainfall intensity, antecedent moisture conditions, and the sequence of rainfall/snowmelt events (Taylor & Howard, 1996; Owor et al., 2009; Dripps & Bradbury, 2009). Moisture conditions in the fall are especially

important for groundwater recharge in the spring, particularly if the soils freeze (Stahli et al., 2001; Iwata et al., 2011; Pittman et al., 2019). If the soils do not freeze completely, then antecedent moisture conditions prior to spring snowmelt are more influenced by midwinter melt events than fall precipitation (Thunholm et al., 1989; Pavlovskii et al., 2019; Pittman et al., 2019).

As with most components of the water cycle, groundwater recharge is highly susceptible to changes in climate. In particular, climate projections predict recharge in snow-dominated regions could increase during the summer months but that spring recharge could decrease, leading to increased susceptibility to summer droughts (Okkonen & Klöve, 2011). A warming climate could also influence frost dynamics, potentially increasing the number of freeze/thaw cycles occurring over the winter and further complicating infiltration into frozen soils (Kane & Stein, 1983; Henry, 2008). Annual recharge is expected to decrease due to a combination of warmer summer temperatures (more water lost to evapotranspiration) and reduced winter precipitation (less water available for spring recharge) (Okkonen et al., 2009).

2.2) Groundwater Dynamics in Formerly Glaciated Systems

Formerly glaciated terrain is often characterized by low permeability glacial tills that overlay low-relief hills and ridges. Due to the method of deposition, glacial tills are typically dominated by silt and clay and exhibit significant heterogeneity and anisotropy. The presence of clay and silt causes groundwater flow through glacial tills to be extremely slow, with reported residence times through tills on the order of thousands of years (Desaulniers et al., 1981; Fortin et al., 1991; Trost et al., 2020). Heterogeneity in tills can exist as sand and gravel lenses, vertical sand dikes, and fractures (Gerber et al., 2001; Van der Kamp & Hayashi, 2009). This heterogeneity has been observed in stable-isotope profiles, hydraulic head profiles, and slug tests (Desaulniers et a.l., 1981; Keller et al., 1988; Gerber et al., 2001; Hendry et al., 2004; Trost et al., 2020). Sand and gravel lenses can exist as extensive sheets which act as *intertill aquifers* and are

an important groundwater resource for communities in formerly glaciated regions (Van der Kamp & Hayashi, 2009).

Despite the low conductivity of the till material, relatively high groundwater flow rates have been observed in glacial tills due to preferential flow pathways (Keller et al., 1988; Fortin et al., 1991). Preferential flow can occur through vertical or horizontal fractures, sand or gravel lenses, or sand dikes (Keller et al., 1988; Fortin et al., 1991; Gerber et al., 2001; Hendry et al., 2004; Cuthbert et al., 2010; Trost et al., 2020). Piezometers installed in tills might intersect these conductive features, which could alter the calculation of hydrogeological properties determined from slug and bail tests (Desaulniers et al., 1989; Keller et al., 1988; Trost et al., 2020). Models of groundwater flow through tills suggest that flow might occur through a stepwise mechanism, with groundwater moving vertically downward through fractures and dikes and then horizontally through sand and gravel lenses (Gerber et al., 2001). Thus, the bulk permeability of glacial tills can often be orders of magnitude greater than the permeability of the till matrix itself (Keller et al., 1988; Gerber et al., 2001; Cuthbert et al., 2010).

Glacial tills are often weathered and oxidized near the surface, leading to an increased permeability relative to deeper, unweathered tills (Fritz et al., 1976; Desaulniers et al., 1981; D'Astous et al., 1989; Hendry et al., 2004; Van der Kamp & Hayashi, 2009). This difference in permeability suggests that groundwater can become perched at the weathered/unweathered interface (Fritz et al., 1976). The weathered zone usually extends less than eight meters down, but weathered zones as thick as 18 meters have been reported (Hendry et al,. 1988; Ruland et al., 1991).

Despite the enhanced bulk permeability of tills due to weathering or preferential flow pathways, infiltration and percolation is still slow. As a result, recharge via direct infiltration of meteoric waters is usually limited to sandier tills (Fortin et al., 1991; Van der Kamp & Hayashi, 1998; Jones & Tomasek, 2015; Pam et al., 2020). Depression-focused recharge in lower-

permeability tills can be enhanced by lateral subsurface flow (Stumpp & Hendry, 2012; Jones & Tomasek, 2015; Pam et al., 2020). This phenomenon is more pronounced when a less permeable layer underlies a more permeable layer, causing a lateral redistribution of percolating water (Weiler et al., 2006; Chifflard et al., 2019; Mohammed et al., 2019).

Typically, water table elevations will mirror surface elevations if recharge is evenly distributed across an area (Freeze & Witherspoon, 1967). However, in clay-rich systems, the uneven distribution of recharge can lead to water tables that are the inverse of surface elevation (Lissey, 1971; Keller et al., 1988; Jones & Tomasek, 2015). These inverted water tables can develop around ponded depressions in the form of water table "mounds" and are more common in weathered till units where bulk permeability is relatively high (Keller et al., 1988). As depressions fill with rain or meltwater, they can transmit water to the surrounding groundwater system through bank storage (Van der Kamp & Hayashi, 2009; Jones & Tomasek, 2015; Hayashi et al., 2016; Pam et al., 2020). Thus, the shallow groundwater systems surrounding depressions can be relatively active and can respond to precipitation events relatively quickly (Jones & Tomasek, 2015; Hayashi et al., 2016). The active groundwater system surrounding a depression is sometimes referred to as the *zone of transmission* or a *transmission aquifer* (Van der Kamp & Hayashi, 2009; Pam et al., 2020). The magnitude and direction of groundwater flow in these zones is dependent on the hydraulic gradient between the depression and the surrounding groundwater system; thus, the magnitude and direction can vary seasonally and spatially (Jones & Tomasek, 2015; Pam et al., 2020). For example, the hydraulic gradient might switch during snowmelt periods such that a recharge depression starts to receive groundwater discharge (Berthold & Hayashi, 2004; Jones & Tomasek, 2015).

Ultimately, not all depressions will focus recharge; the influence of depressions on shallow groundwater systems depends on their topographic position (Berthold & Hayashi, 2004; Hayashi et al., 2016). Depressions in a higher topographic position may focus recharge, but this

recharge might be discharged to depressions in a lower topographic position (Figure 2.2). During periods of large surface runoff, such as snowmelt, depression storage may be exceeded and a "fill-and-spill" network can develop between depressions (Figure 2.2; Hayashi et al., 2003; Van der Kamp & Hayashi, 2009; Shaw et al., 2012). The ability of a ponded depression to focus recharge might also depend on its permanence and its hydrologic connection to other depressions (Pam et al., 2020).

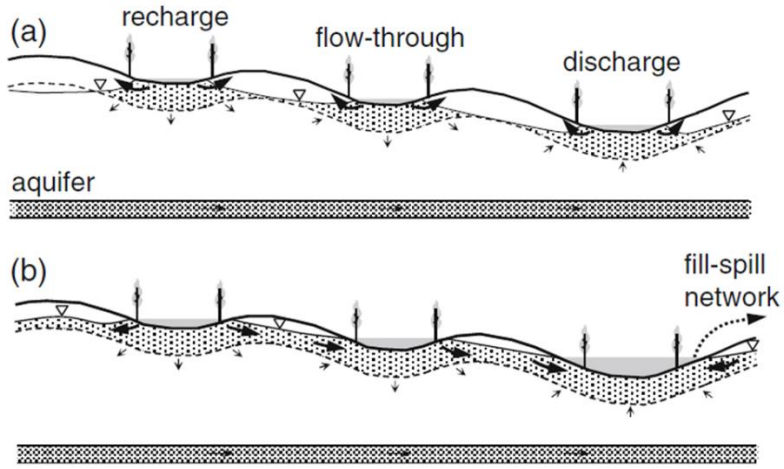

Figure 2.2: Schematic of recharge ponds and discharge ponds in a prairie wetland system underlain by an intertill aquifer during (a) normal conditions and (b) fill-and-spill conditions. Dotted areas represent the transmission zone surrounding depressions. From Van der Kamp & Hayashi, 2009.

While the depression-focused recharge model is well-documented, its role in recharging deeper groundwater systems is less certain. This is compounded by the fact that "recharge" can be hard to define conceptually in lower-permeability systems. Depressions that collect and subsequently transmit runoff can recharge shallow groundwater systems but this recharge "pulse" might be entirely dissipated laterally or lost to evapotranspiration before it can percolate downward (Keller et al., 1988; Hayashi et al., 2016). Thus, estimates of recharge near depressions may be inaccurate or misleading (Jones & Tomasek, 2015). Deeper recharge to intertill aquifers is minimal, with reported rates on the order of millimeters to centimeters per year (Desaulniers et al., 1981; Hayashi et al., 2016; Pam et al., 2020). Surface water management practices such as

irrigation will likely have a minimal effect on deeper recharge since it is already very limited (Keller et al., 1988). Runoff diversion (e.g., tile drainage) may impact shallow groundwater recharge as it could divert water away from depressions (Keller et al., 1988; Hayashi et al., 2016).

2.3) Influence of Soil Frost on Groundwater Processes

In general, frozen soils will delay or reduce infiltration due to the blocking of pore spaces by ice (Kane & Stein, 1983; Pomeroy & Brun, 2001; Stahli et al., 2001; Okkonen & Klove, 2011; Pittman et al., 2019). This ice-blocking leads to reduced permeability, infiltration capacity, and hydraulic conductivity in frozen soils. In reality, however, frozen soils are not entirely impermeable (Burt & Williams, 1976). The permeability of frozen soils depends on a variety of factors such as frost depth, water content prior to freezing, and soil texture and temperature (Kane & Stein, 1983; Watanabe et al., 2012; Lundberg et al., 2015; Pittman et al., 2019).

Snow depth is the key parameter when assessing how deep a soil frost will develop; generally, snow depth is inversely proportional to frost depth (Pomeroy & Brun, 2001; Hardy et al., 2001). However, the extent and duration of subzero temperatures, soil texture, and initial soil water content also influence frost depth (Benoit & Bornstein, 1970). Frost depth is generally greater in coarser-grained soils that are relatively dry prior to freezing. Soils that are relatively wet prior to freezing are more likely to form *concrete frost*, in which most of the soil pore space is occupied by ice (Pomeroy & Brun, 2001). Concrete frost restricts infiltration more than *granular frost*, which occurs when there is still a significant amount of pore space occupied by air or liquid water. Ice lenses, even when thin, can also impede infiltration (Iwata et al., 2011). These ice lenses are more likely to form in wetter soils, but can also form at the base of the snowpack (Kane & Stein, 1983). Thus, frost depth alone is not a good quantification for the effects that soil frost has on infiltration (Jansson & Gustafsson, 1987).

Infiltration into frozen soil is shown to be inversely proportional to soil water content prior to freezing (Kane & Stein, 1983; Pittman et al., 2019). Wetter frozen soils exhibit slower infiltration rates than drier frozen soils and are often considered impermeable (Figure 2.3; Kane & Stein, 1983; Pomeroy & Brun, 2001; Kane & Stein, 1983; Watanabe et al., 2012). As a result, wetter frozen soils promote greater runoff generation (Kane, 1980; Espeby, 1990; Shanley & Chalmers, 1999; Hardy et al., 2001; Pomeroy & Brun, 2001; Stahli et al., 2001). Drier frozen soils exhibit significant infiltration capacities due to a larger portion of air-filled pores (Burt & Williams, 1976; Johnsson & Lundin, 1991; Stahli et al., 2001; Pittman et al., 2019). Infiltration into unsaturated soils is thus largely dependent on the ice content in the upper reaches of the soil (Kane & Stein, 1983; Granger & Gray, 1984; Gray et al., 1985; Pomeroy & Brun, 2001).

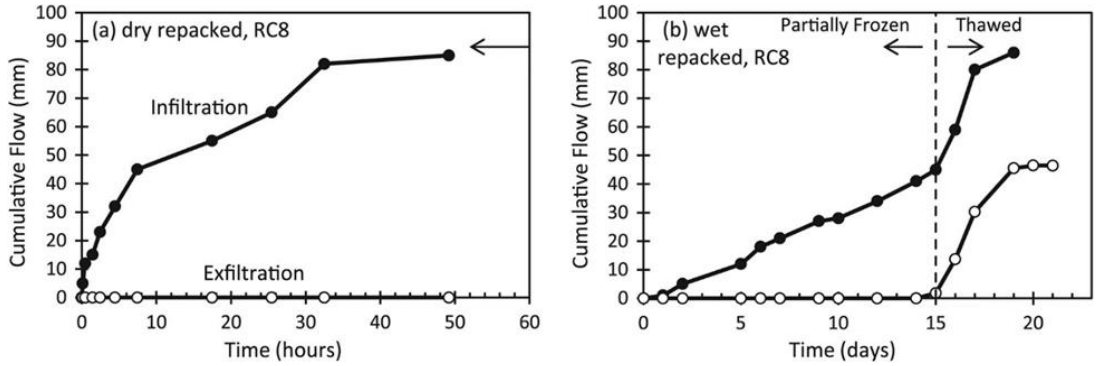

Figure 2.3: Experimental results of infiltration and exfiltration in frozen, repacked (non-macroporous) soil columns that were (a) dry before freezing ($\theta_i < 0.20$) and (b) wet before before freezing ($\theta_i > 0.40$). Note the difference in time scales. From Pittman et al., 2019.

Given the influence of water content on infiltration into frozen soils, midwinter melt events can have significant influence on snowmelt infiltration in the spring. Under dry antecedent moisture conditions, the first midwinter melt event can result in relatively large amounts of infiltration (Pittman et al., 2019). Once snowmelt infiltrates, it can refreeze and restrict further infiltration (Thunholm et al., 1989; Watanabe & Kugisaki, 2017). Recurring melting and freezing can result in increasingly wetter soils prior to each freeze, increasingly restricting infiltration for later events (Iwata et al., 2011; Mohammed et al., 2019; Pittman et al., 2019; Pavlovskii et al.,

2019). This effect can be pronounced during the diurnal cycle of snowmelt in which meltwater infiltrates during the day and refreezes at night (Nyberg et al., 2001).

Snowmelt infiltration through frozen soil has been observed in several field studies as a result of preferential flow through macropores (Jansson & Gustafsson, 1987; Thunholm et al., 1989; Johnsson & Lundin, 1991; Daniel & Staricka, 2000; Stahli et al., 2001; Mohammed et al., 2019). These macropores form from rootholes, animal burrowing, or cracks and fractures due to desiccation and weathering (Bevin & Germann, 1982). In finer-grained soils, fractures can also form during soil freezing and thawing (Pawluk, 1988; Weigert & Schmidt, 2005). Unless the soil is at or close to saturation when freezing, these macropores remain air-filled as the soil freezes and provide a conduit for meltwater movement (Espeby, 1990; Thunholm et al., 1989; Watanabe & Kugisaki, 2017). Drier frozen soils can also transmit water through air-filled pores within the soil matrix itself (Espeby, 1990; Pittman et al., 2019). Macropore flow is governed by different physical processes than matrix flow; while dual-domain models have captured these different flow mechanisms well for unfrozen soils, these models need refinement to account for frozen soil conditions (Mohammed et al., 2018). Overall, the effects of preferential flow through frozen soils on deeper groundwater processes is still poorly understood (Mohammed et al., 2019).

The infiltration capacity of frozen soil is influenced by frost depth, antecedent moisture conditions, soil texture, and the presence of macropores; therefore, these parameters also influence the partitioning of snowmelt infiltration and surface runoff. This partitioning is particularly important in low-permeability systems that rely on depression-focused recharge (Baker and Spaans, 1997; Van der Kamp & Hayashi, 1998; Sharratt, 2001). Snowmelt-driven surface runoff is routed to depressions, but subsequent infiltration and recharge can be delayed by soil frost. However, water ponded in depressions can store a significant amount of heat that can be transmitted to the underlying frozen soil, which allows the thawing front to advance quicker under depressions (Hayashi et al., 2003). In addition, macropore flow is an important mechanism

in facilitating depression-focused recharge through frozen soil (Baker & Spaans, 1997; Sharratt, 2001; Mohammed et al., 2019). This is likely due to the enhanced role of macropore flow in wetter frozen soils that would be found underneath depressions (Espeby, 1990; Pittman et al., 2019). Since depression-focused recharge is more pronounced when infiltration is limited (and thus more runoff is generated), it acts as a significant mechanism through which snowmelt can bypass the frozen soil matrix.

Despite the influence of soil frost on infiltration processes relevant to groundwater recharge, most common recharge estimates do not include a soil frost component or account for infiltration into frozen soils (Okkonen & Klove, 2011; Lundberg et al., 2015). Groundwater-surface water interaction models also struggle to simulate the timing of recharge due to a lack of a soil frost component (Okkonen & Klove, 2011). Thus, many of these recharge estimates may not be accurate in colder regions that experience seasonally-frozen ground. Modelling of frozen soil processes can be difficult due to the coupled energy and mass transfer that occurs within a freezing/thawing soil (Stahli et al., 2001). Frost dynamics within a single soil profile have been simulated well by empirical and analytical models (Zhao & Gray, 1999; Okkonen & Klove, 2011; Heinze & Blocher, 2019). However, watershed-scale applications of these models have not yielded the same success (Lundberg et al., 2015). In general, the effect of soil frost on infiltration can vary with scale, usually having a stronger influence in smaller-scale studies (Shanley & Chalmers, 1999; Lundberg et al., 2015). As a result, field-scale models of infiltration into frozen soil can deviate substantially from actual field observations (Johnsson & Lundin, 1991; Stahli et al., 2001).

2.4) Stable Isotopes in Groundwater

$\delta^{2}H$ and $\delta^{18}O$ act as conservative tracers in the shallow subsurface (Clark & Fritz, 1997) and can thus be used to estimate sources of groundwater recharge, recharge rates, subsurface flow pathways, and residence times of groundwater (Saxena, 1984; Gerber et al., 2001; O'Driscoll et

al., 2005; McConville et al., 2005; Adomako et al., 2010; Stumpp & Hendry, 2012). Seasonal variations in the isotopic composition of precipitation can thus be conserved and flow pathways can be traced by obtaining shallow groundwater samples (Clark & Fritz, 1997; O'Driscoll et al., 2005; Earman et al., 2006; Adomako et al., 2010).

Stable water isotopes can be used to estimate groundwater recharge rates using peak-shift methods (Saxena, 1984; McConville et al., 2005; Adomako et al., 2010). These methods rely on seasonal peaks in the isotopic composition of precipitation being conserved near the top of the soil column. Some peak-shift methods determine recharge rates based on the isotopic shift between precipitation and soil water. Mean water flux (i.e., recharge) can be calculated as:

$$\bar{q} = \frac{\int_0^{Z_p} \theta(z)dz}{\Delta t_p} \tag{2.1}$$

where $\bar{q}$ is the mean water flux, θ is the water content of the soil, Z_p is the depth of the isotope peak in the soil, and Δt_p is the time duration between the isotopic peak in precipitation and the isotopic peak in soil water (Adomako et al., 2010). Other peak-shift methods are based on isotopic shifts between successive shifts in soil water. Recharge rate is calculated as:

$$R = (\theta - \theta_f)\Delta Z \tag{2.2}$$

where R is the recharge rate, θ is the average soil moisture content between the two peaks, θ_f is the field capacity, and ΔZ is the difference in depth between the two peaks (McConville et al., 2005). The time difference between isotopic peaks in precipitation and soil water can also indicate residence times in the soil column (O'Driscoll et al., 2005). Peak-shift methods are typically only accurate under certain conditions specific to the soil properties and topography of an area (Chesnaux & Stumpp, 2018). These methods rely on how well seasonal signals are distributed and conserved and thus are more applicable in temperate climates with homogenous soils.

Studies attempting to identify sources of recharge rely on binary end-member mixing analysis or by plotting samples against the Global Meteoric Water Line (GMWL) (Winograd et al., 1998; Lee & Kim, 2006; Adomako et al., 2010; Pavlovskii et al., 2018). The GMWL represents the observed linear relationship between δ^2H and $\delta^{18}O$ in waters at the global scale (Figure 2.4; Craig, 1961). Different sources of water (e.g. groundwater, precipitation, streamflow) and waters from different regions will plot at different points along the GMWL. Local meteoric water lines (LMWLs) deviate from the GMWL, both in slope and in δ^2H intercept, and can vary by season (Clark & Fritz, 1997). This allows inferences to be made about seasonal contributions to groundwater recharge (Lee & Kim, 2006).

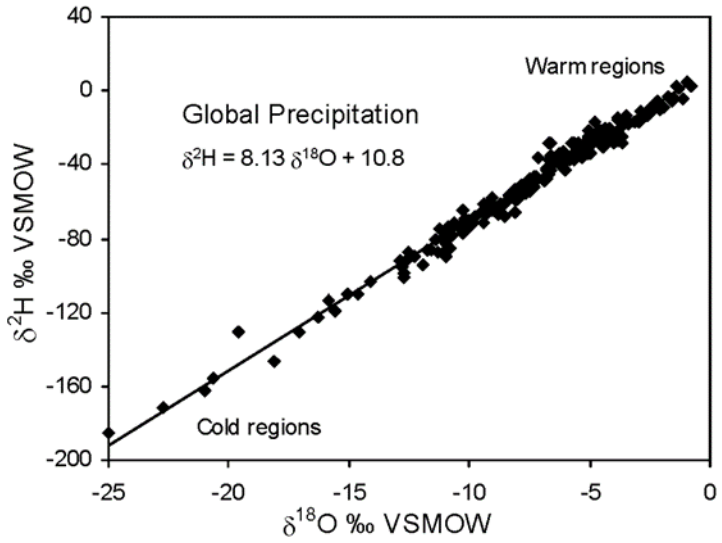

Figure 2.4: The Global Meteoric Water Line for precipitation. From Clark & Fritz, 1997.

End-members can be difficult to determine for different sources of recharge, particularly snowmelt. There can be a notable difference between the isotopic composition of fresh snow and the bulk meltwater derived from it due to the fractionation caused by snowpack metamorphism (Earman et al., 2006; Pavlovskii et al., 2018). Additionally, there can be significant spatial variability in the isotopic composition of a snowpack over short distances, particularly during snowpack depletion (Pavlovskii et al., 2018). Thus, fractionation processes within a snowpack

and spatial variability should be considered when attempting to quantify the contribution of snowmelt to groundwater recharge.

Stable isotopes have also been used in studies of groundwater movement through glacial tills (Gerber et al., 2001; Hendry et al., 2004). As water percolates through till aquitards, a steady depletion of heavier isotopes is expected unless the water is able to bypass the till matrix (Desaulniers et al., 1981). Several studies have noted no depletion of isotopic signature, which indicates preferential flow through macropores, fractures, or high-permeability features such as sand lenses (Gerber et al., 2001; Hendry et al., 2004; O'Driscoll et al., 2005; Mueller et al., 2014). Other glacial till studies have estimated groundwater residence times through till aquitards using tritium (^{3}H), an isotope of hydrogen known to be formed from nuclear events in the 1950s (Desaulniers et al., 1981; Gerber et al., 2001; Trost et al., 2020). Since the formation of tritium was relatively recent, the presence of tritium can indicate how recently deeper intertill aquifers have been recharged.

More recently, stable isotopes have been used to investigate snowmelt infiltration and the role of depression-focused recharge in glacial tills (Fortin et al., 1991; Stumpp & Hendry, 2012; Mueller et al., 2014; Pam et al., 2020). Most studies involving stable isotopes in this manner are qualitative and used in the development of conceptual models (Chesnaux & Stumpp, 2018). Fractionation can occur at several different stages during depression-focused recharge, which makes it more difficult to quantify using stable isotopes (Pavlovskii et al., 2018). Most of this fractionation occurs as the snowpack or ponded water is exposed to the atmosphere, although fractionation can also occur during runoff generation. Enrichment in surface runoff can occur based on two observations: (1) isotopically depleted meltwater gets released early during snowmelt and (2) preferential flow into frozen soil can occur until the ground becomes mostly saturated with meltwater and ice. This leads to potential enrichment of meltwater-derived surface runoff relative to snowpack composition (Pavlovskii et al., 2018).

The use of stable isotopes in studies of groundwater recharge provides valuable insight but comes with limitations. The seasonal variation of precipitation is generally attenuated as water percolates through the unsaturated zone, and the signal is completely lost below point known as the critical depth (Figure 2.5; Clark & Fritz, 1997; de Vries & Simmers, 2002; O'Driscoll et al., 2005). This is due to the dispersive mixing of infiltrating water with residual pore-water or from evaporation of groundwater close to the soil surface (O'Driscoll et al., 2005). The critical depth is dependent on soil texture and vegetation cover and could vary annually in some regions depending on antecedent moisture conditions, particularly in clay-rich soils (O'Driscoll et al., 2005). This attenuation could be problematic for studies of groundwater-streamflow dynamics in slower-draining watersheds due to the seasonal variation being lost along a flow path before groundwater is able to discharge to streams and/or springs.

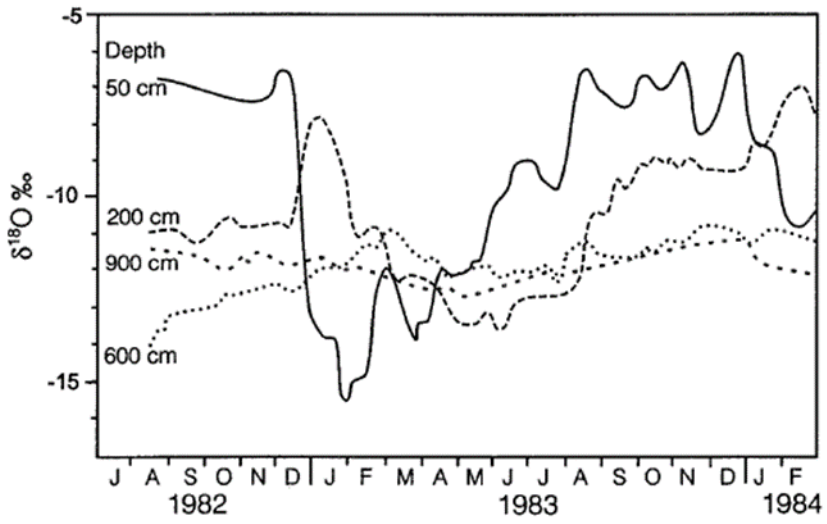

Figure 2.5: Attenuation of δ ^{18}O signal with depth over two years in gravel near Munich. From Eichenger et al., 1984.

Chapter 3: Site Description

3.1) Site history

This study was conducted at the University of Minnesota Duluth's Research and Field Studies Center (RFSC), a 114 km^2 research site at the northeastern end of Duluth, Minnesota (Figure 3.1). The site is approximately 5 km inland from Lake Superior and is at an average elevation of 360 m above sea level (ASL) and approximately 176 m above the surface of Lake Superior. The specific site was located north of the East Branch of Amity Creek, with approximately 10 m of relief sloping downward towards the creek. The field site contained several topographical depressions within a shallow valley (hereafter referred to as the "swale"), with approximately 1.5 m of relief from the center of the field to the outer reaches of the valley. The site was selected due to its accessibility, well-documented research history, and proximity to East Amity Creek.

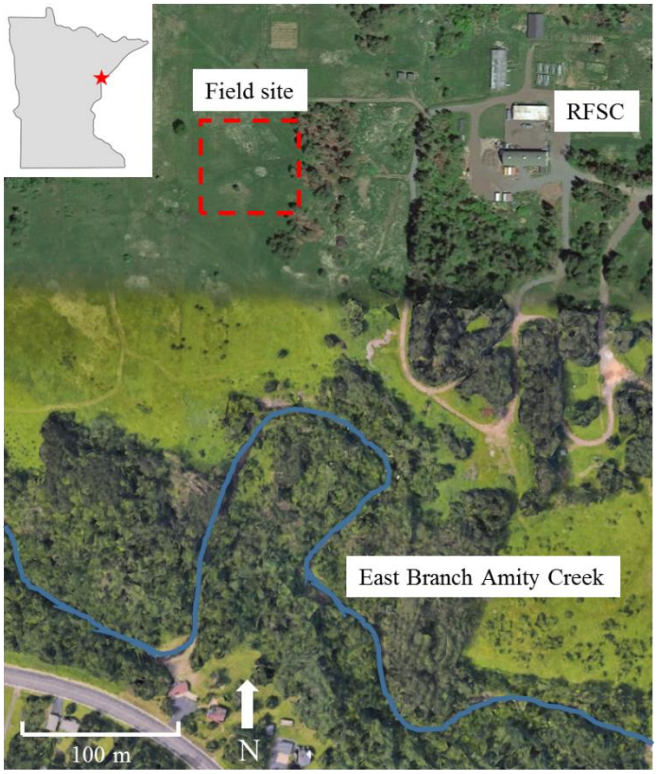

Figure 3.1: Map of field site in relation to the UMD RFSC and the East Branch of Amity Creek.

The RFSC served as an agricultural research station until the mid-1970s, which has implications for soil characteristics and drainage networks at the site. In particular, previous tilling in the area likely resulted in enhanced infiltration at the soil surface. The vegetation in the field was dominated by invasive tansy (*Tanacetum vulgare*), with few native prairie species. The United States Department of Agriculture (USDA) reports that the rooting depth of *T. vulgare* can be as high as 130 cm but is more commonly around 60 cm (Gucker, 2009). In addition to tilling, drain tiles were installed extensively at the site in 1915 and 1929 (Figure 3.2). The tiles were likely installed to drain the area to the north of the site and reroute the drainage south towards East Amity Creek (Figure 3.1; Figure 3.2). However, the full spatial extent of these tiles was unclear. A report from the RFSC published in 1954 noted that the tile had unspecified negative consequences and that "adequate tile drainage in these type soils would be too expensive" (Thompson, 1954). More details on the tilling and drain tiles are provided in the following sections on soils and groundwater dynamics at the site.

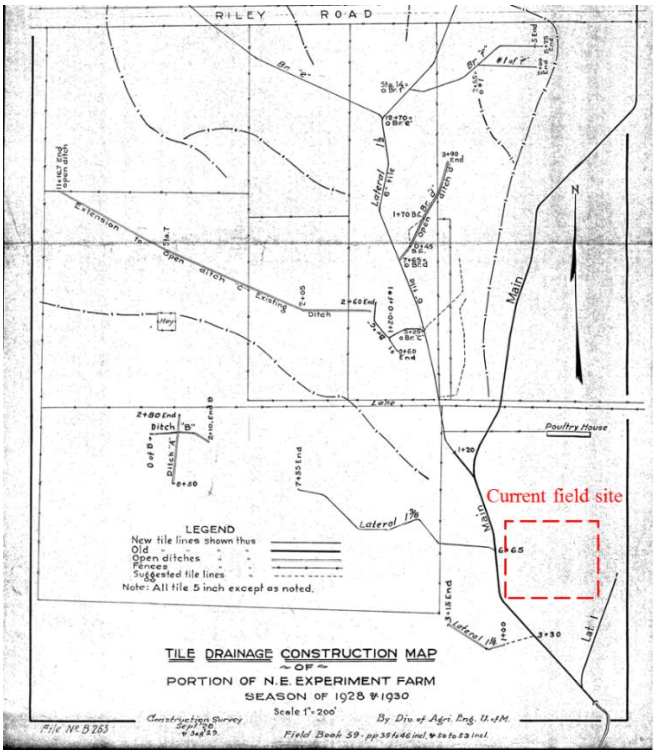

Figure 3.2: Tile drainage construction map published in 1930 with the current location of the field site. From Thompson (1954).

3.2) Climate

The proximity of Lake Superior to the field site results in a combination of continental and maritime climate attributes; the climate is defined as warm-summer humid continental according to the Köppen Climate Classification system. Based on historical data from the nearby Duluth International Airport, the area received an average of 789 mm of rainfall and 2180 mm of snowfall annually over the last 30 years (1990 – 2020); the area usually received the most rain in June, August, or September and the most snow in December, January, or February (Duluth International Airport, NOAA). The mean daily air temperature from 1990 – 2020 was 4°C; the coldest temperatures usually occurred in January (mean = -11.5°C) and the warmest temperatures usually occurred in July (mean = 19.2°C).

3.3) Geology and Soils

The underlying geology in the area consisted of glacial till atop very old (~1.1 billion years) bedrock. The bedrock was Keweenawan-aged igneous rocks of the North Shore Volcanic Group and Duluth Complex. The till had a highly variable thickness (with bedrock being exposed in some areas), was not well-mixed, and was dominated by silt and clay. The till partially filled in the bedrock relief to create a modern landscape of modest-relief hills and ridges with relatively thin layers of soil. Soils within the study site were mostly Alfisols. They were classified as Hydrologic Soil Group D, meaning they are characterized by high clay content, a slow rate of water transmission, high water tables, and high runoff potential. Particle size analyses were performed on the upper meter of the soil using the hydrometer method (Gee & Bauder, 1986). These analyses determined there was a thin (30 cm) layer of sandy loam at the surface of the soil (Appendix 1). Beneath this sandy loam layer, the dominant soil texture was loam or silt loam (Appendix 1). Infiltration tests were conducted using a Turf-Tec Infiltrometer at the soil surface and at 40 cm depth, which demonstrated the enhanced infiltration capacity of the surficial soil relative to the deeper soil. Below 30 cm, the infiltration capacity of the soil decreased

substantially as a result of higher clay content (Appendix 1). Slug tests performed on piezometers (installed at a depth of three meters; see Chapter 4) determined the hydraulic conductivity of the deeper soil to be on the order of 10^{-8} m/s. This value is near the middle of the six-order-of-magnitude range for glacial till reported in the literature (Heath, 1983).

3.4) Groundwater Dynamics

Shallow groundwater processes at the site were influenced by the presence of century-old drain tiles running underneath and upstream of the field site (Figure 3.3). Due to the low hydraulic conductivity of the glacial till, the drain tile acted as a narrow, shallow, semi-confined aquifer. This semi-confined aquifer had an associated potentiometric surface that rose above the land surface slightly north of the field site, resulting in a flowing artesian well that discharged shallow groundwater at the surface (Figure 3.3). The potentiometric surface likely rose above the surface at the discharge point due to the drain tile collapsing, a common occurrence for early 20^{th} century drain tiles (Minnesota Groundwater Association, 2018). The water discharged at this point had a steady temperature between 7°C and 9°C throughout the year (as measured between July of 2020 and January of 2021). Downstream of this discharge point, a combination of discharged water and continued upward leakage from the drain tile filled in various topographic depressions along the swale running through the center of the field site.

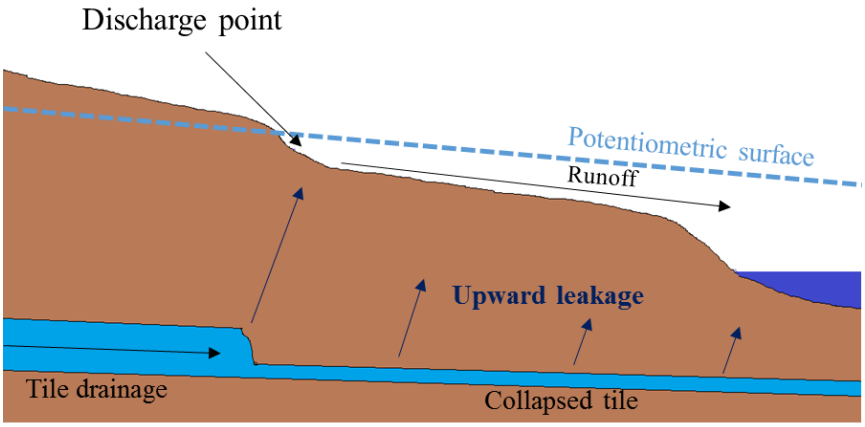

Figure 3.3: Illustration of the collapsed drain tile and the resulting leakage being routed to downstream surface depressions.

The discharge from the drain tile formed permanent ponds in the swale that would likely otherwise have been more ephemeral in nature. Other surface depressions at the field site located along the hillslope (outside of the influence of the drain tile) filled with water following rainfall or snowmelt but subsequently dried out. The permanence of the ponds within the swale led to the formation of an inverted water table (i.e., a water table mound), similar to that surrounding a losing stream. Thus, this water table mound served as the local water table at the field site and controlled the direction of groundwater flow throughout the year. The low topography of the hillslope adjacent to the swale allowed shallow groundwater to move laterally, away from the swale throughout most of the year (i.e., the swale acted a "losing" water body); in effect, most of the year, shallow groundwater moves in a direction opposite to the direction of surface runoff. This kept the soil in the surrounding margins much wetter throughout the year. It is unclear how the system drained prior to installation of the drain tiles; however, the swale never dried out during this study, illustrating that the system never drained completely. This ultimately affected the system response to rainfall and snowmelt, which is discussed in more detail in Chapter 6.

Chapter 4: Methods

Continuous monitoring of shallow groundwater levels, soil moisture, soil temperature, and streamflow were required to assess the fate and transport of rainfall and snowmelt at the field site. Soil moisture and shallow groundwater responses to rainfall and snowmelt were analyzed to assess the timing of infiltration, percolation, and recharge. Additionally, stable water isotopes from different components of the hillslope-swale system were analyzed to provide insight into the pathways and timing of shallow groundwater movement following rainfall or snowmelt events.

The field site consisted of three monitoring locations positioned along a hillslope transect: an upslope, midslope, and downslope site (Figure 4.1). The hillslope relief was moderate, with roughly 1.5 meters of elevation difference across the 40 meter transect sloping west. The downslope site was located approximately 8 meters from a large depression within the swale, which was continuously supplied with water from the collapsed drain tile to the north (see Chapter 3).

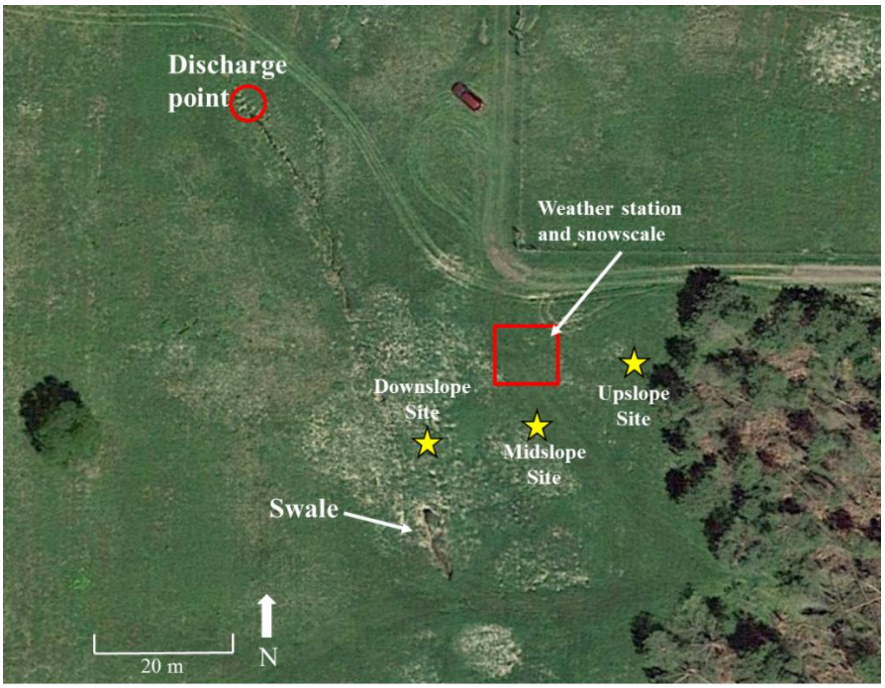

Figure 4.1: Map of the field site detailing the locations of the monitoring sites, drain tile discharge point, and the swale.

4.1) Instrumentation

Climate Data

A HOBO Onset weather station previously installed at the site continuously measured air temperature (S-TBH-M002 sensor) and barometric pressure (S-BPB-CM50 sensor) at five-minute intervals throughout the duration of the study (Figure 4.1). The weather station also included a tipping-bucket gauge (S-RGB-M002) that provided precipitation data at five-minute intervals throughout the study (2019-2021). To assess long-term trends in precipitation and temperature, additional weather data were obtained from the National Oceanic and Atmospheric Administration (NOAA) at the Duluth International Airport, located approximately eight miles west-southwest of the study site. Snowpack depth and snowfall data were also acquired from the Duluth International Airport.

A Snow Scale SSR from Sommer Messtechnik that was previously installed at the site was used to track snowpack snow-water equivalent (SWE) (Figure 4.1). The snow scale consisted of an array of load-bearing plates that continuously measured the weight of the overlying snowpack and converted it to a SWE value in mm. The snow scale collected measurements every 15 minutes during periods of snow cover. Battery issues prevented any reliable data from being obtained for most of the 2019-2020 winter, but thorough data were obtained for the 2020 snowmelt season, the 2020-2021 winter, and the 2021 snowmelt season.

Shallow Groundwater Dynamics

To monitor groundwater levels, piezometers were installed at each site in July 2019. The piezometers were constructed with 2” schedule 40 PVC installed to a depth of three meters, which included a 15 cm screen at the base of the piezometer. The base of the borehole (near the well screen) was back-filled with sand, and the rest of the borehole was back-filled with bentonite clay pellets. HOBO Onset pressure transducers (U20L-04) were placed in the bottom of each

piezometer in September 2019 that continuously monitored absolute pressure and water temperature at ten-minute intervals. Absolute pressure measurements were subsequently converted to water level using barometric pressure data from the weather station according to the following equation:

$$h_w = (P_{abs} - P_{atm}) * 10.332 \quad (4.1)$$

Where P_{abs} is the absolute pressure measured by the transducer, P_{atm} is the atmospheric pressure measured by the weather station, and h_w is the height of the overlying water column in meters. Both absolute pressure and atmospheric pressure are in units of atmospheres (atm). The piezometer at the upslope site was continuously dry throughout the duration of the study; thus, the water table was below a depth of 3 meters at the upslope site from September 2019 to April 2021.

I removed 24 hours of piezometer data following every sampling event due to the direct effect that sampling had on water levels. I also removed 72 hours of data from March 24th to March 26th in 2020 following the purging of the piezometers on March 23rd.

Soil Moisture and Temperature

To monitor soil water content, soil moisture sensors from Campbell Scientific (CS650) and Truebner (SMT100) were installed at each monitoring site. Both types of sensors utilized the dielectric method to calculate volumetric water content (VWC) at ten-minute intervals. In addition to VWC, each sensor also recorded soil temperature in °C at ten-minute intervals throughout the duration of the study. The sensors were installed by digging holes to a depth of one meter at each of the three study sites. Each sensor was installed horizontally into the soil face at depths of 15, 50, and 100 cm, and two sensors were installed at each depth at each site (Figure 4.2). Due to issues with water-logging during installation, sensors were only installed to depths of 15 and 50 cm at the downslope site. Truebner sensors were installed at the upslope and downslope sites and a mix of Truebner and Campbell Scientific sensors were installed at the

midslope site. All sensors were installed by October 1st, 2019. Truebner sensors were connected to EnviroDIY Mayfly dataloggers and Campbell Scientific sensors were connected to a Campbell Scientific datalogger (CR1000X).

There were several issues with obtaining reliable data from every sensor. Wiring issues and animal damage only allowed me to obtain data from one sensor at each depth at the upslope and midslope site. Due to unknown coding issues, the sensors at the downslope site only logged data sporadically and thus did not yield reliable data. In total, soil moisture data were limited to six sensors: one sensor at 15, 50, and 100 cm depth at both the upslope and midslope site. Initial coding issues with the upslope site prevented any data from being obtained prior to August 2020 and thus soil moisture data from fall 2019 and spring 2020 were limited to the midslope site. During data processing, nonsensical data points were removed from the VWC time-series such as values higher than 1.00. These types of values were sporadic and isolated such that no large portions of data were ever removed.

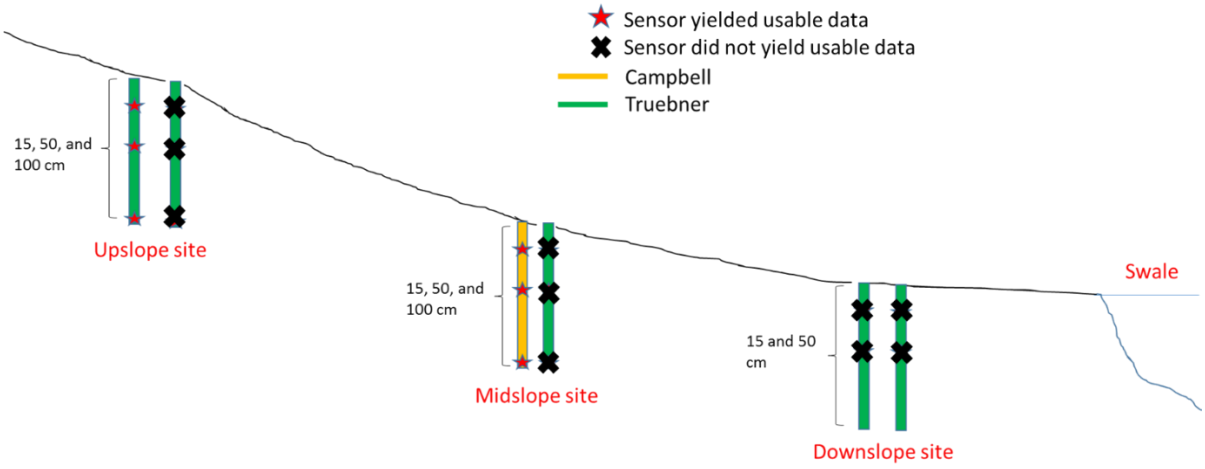

Figure 4.2: Soil moisture sensor distribution at the upslope, midslope, and downslope sites.

Stream Discharge

To monitor stream stage and streamflow, a stream gauge was installed in the East Branch of Amity Creek, directly south of the field site, in July 2019. The stream gauge was constructed using 1" schedule 40 PVC and a HOBO Onset pressure transducer (U20-001-04-Ti). The transducer was fastened to the PVC using zip-ties and the bottom 10 cm of the PVC was slotted to allow for good ventilation and contact with the surroundings. The PVC was attached to a piece of rebar using zip-ties and hose clamps and the rebar was pounded 40 cm into the streambed such that the transducer was positioned at the base of the water column (Figure 4.3). The transducer continuously measured absolute pressure at ten-minute intervals, which was subsequently converted into stream stage and discharge (see Equation 4.1).

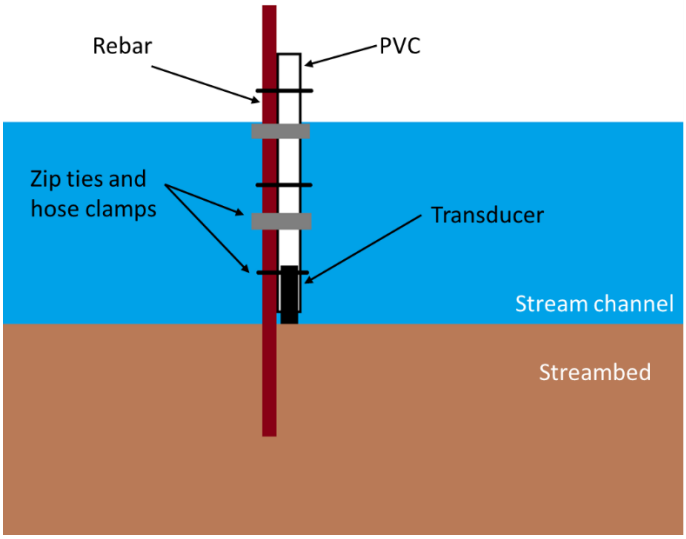

Figure 4.3: Schematic of stream gauge construction and installation.

Soil Water Sampling

In order to collect soil water samples for isotopic analysis, suction lysimeters were installed at depths of 40 cm at each site in November 2019. To better assess the soil water near the soil surface and to compare soil water at different depths, additional lysimeters were installed

at a depth of 15 cm at each site in August 2020. Each lysimeter consisted of a porous ceramic cup fastened to 2" schedule 40 PVC and capped with a rubber stopper. Each lysimeter had two tubes running through the rubber stopper and into the lysimeter such that a vacuum could be applied and samples could be drawn (Figure 4.4). Soil obtained from the borehole during digging was mixed with silica flour and deionized water to create a slurry that was poured into the borehole. The purpose of the slurry was to enhance hydrologic connection between the ceramic cup and the surrounding soil, and enough slurry was poured to completely submerge the ceramic cup. The rest of the borehole was back-filled with bentonite clay pellets. The lysimeters were installed at an angle to minimize interference from precipitation and to prevent water drainage and ponding around the borehole.

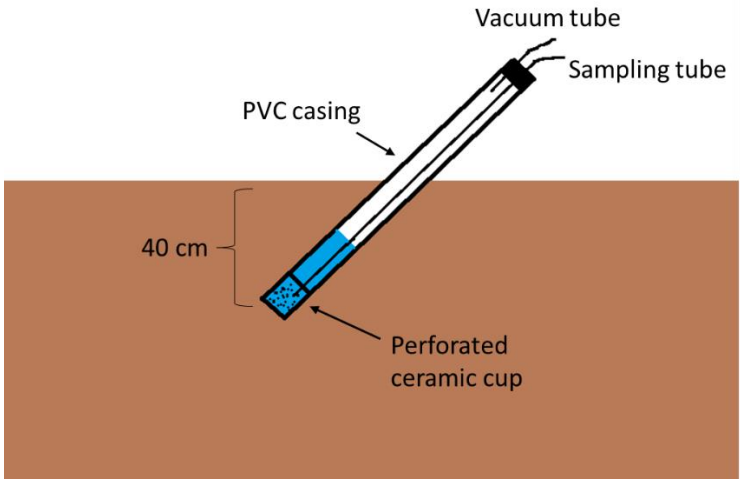

Figure 4.4: schematic of lysimeter construction and installation.

4.2) Sampling Protocol

Periodic water samples were collected from the swale, East Amity Creek, piezometers, and lysimeters for stable water isotope analysis. Precipitation (rain and snow) and snowpack

samples were also collected from the field site throughout the duration of the study. During the spring snowmelt, samples were collected daily from the swale, East Amity Creek, lysimeters, and snowpack. Because pumping for water samples altered the water levels in the piezometers, groundwater samples were collected biweekly during the snowmelt and post-melt periods. Throughout the summer growing season, fall, and winter, samples from the swale, East Amity Creek, and lysimeters were collected weekly, with piezometers sampled bi-weekly.

A peristaltic pump (Masterflex L/S Portable Sampler) was used to collect samples from the piezometers. Typically, groundwater wells should be purged two to three times before collecting a sample. The midslope and downslope piezometers were purged during the snowmelt season in 2020 prior to collecting the first water sample, but both piezometers took several days to fully recover. Due to this slow recovery time and the reliance on water level data, the wells were not purged prior to sampling for the rest of the study.

Precipitation samples were collected directly from a rain gauge installed at the field site on an event basis throughout the duration of the study. The samples were collected as close to the end of the rain event as possible to minimize the evaporative effects on the isotopic composition of the samples. Rain samples that were suspected of being exposed to significant evaporation (e.g. the rain gauge had been in direct sun for multiple hours before collection) were not included in the analysis.

A Federal snow sampling tube from Geoscientific was used to collect depth-integrated snow samples. I collected and homogenized samples from three different locations at the site to obtain a spatially-averaged sample. I collected snow samples weekly during times of snow cover. During snowmelt periods, snow samples were collected daily.

4.3) Data Analysis

Water Delivery Responses

A response in soil moisture to incoming water (i.e. precipitation or snowmelt) was defined using an increase (percent change) of at least 2% volumetric water content (VWC) from the preceding time-step:

$$\%\ Change = \frac{(\theta_t - \theta_{t-1})}{\theta_{t-1}} \tag{4.2}$$

Where θ_t is the volumetric water content at time t and θ_{t-1} represents the volumetric water content at the previous time-step. An increase of 2% VWC (or 0.02 cm^3/cm^3) was selected to eliminate increases that were associated with instrument noise (sensor accuracy was 2% for both the Campbell and Truebner sensors). Percent change was investigated at time steps of one day to better relate soil moisture response to stable isotope samples from the lysimeters, which were collected on a daily basis. Responses in piezometers were defined similarly, although the threshold for a response was a 4% change at a time-step of one day. Following data processing, time-series data for piezometers, soil water content, and streamflow were aggregated up to daily averages. Rainfall data were aggregated up to daily sums.

Measuring Stable Isotope Composition

Water samples were analyzed at the Large Lakes Observatory in Duluth using a Picarro L2130-I cavity ring down mass spectrometer. Values of $\delta^{18}O$ and $\delta^{2}H$ were obtained by comparing the isotopic ratios of heavy (^{18}O and ^{2}H) and light (^{16}O and ^{1}H) isotopes to the Vienna Standard Mean Ocean Water (VSMOW) reference using the following equation:

$$\delta = \left(\frac{R_{sample}}{R_{standard}} - 1\right) x\ 1000‰ \tag{4.3}$$

Where *R* is the ratio between heavy and light isotopes (e.g., $^{18}O/^{16}O$) and δ is the relative difference of isotopic ratios between the sample and the standard. Values of $\delta^{18}O$ and $\delta^{2}H$ were plotted in dual-isotope space against the global meteoric water line (GMWL) obtained from Craig (1961):

$$\delta^2 H = 8.0\delta^{18} O + 10.0 \quad (4.4)$$

and the local meteoric water line (LMWL) obtained from Jasperson et al (2018):

$$\delta^2 H = 8.4\delta^{18} O + 15.5 \quad (4.5)$$

Estimation of Saturation

I estimated saturation values for soils at different depths at each monitoring site using methods presented by Chandler et al. (2017), which estimated saturation as the maximum observed value of volumetric water content (VWC) in a ten-minute frequency distribution of the data. This method was selected due to its relation to the soil moisture sensors themselves. Soil texture methods for determining soil saturation would have been based on soil samples collected for particle size analysis, which were collected at a significant distance from the soil moisture sensors so as to not disturb the soil. To ensure that the maximum observed value was a valid measurement and not instrument noise, values were only considered if they had a frequency of 100 or greater. This estimation method relies on time-series data that are sufficiently long (one year of data is recommended) and thus there was more uncertainty in values estimated for the upslope site, which only had data for seven months. Saturation data, as well as frequency distribution data, is presented in Appendix 1.

Estimation of Snowmelt Infiltration

I estimated snowmelt infiltration according to the empirical model presented by Gray and Landine (1985):

$$I = 5(1 - S)SWE^{0.584} \quad (4.6)$$

Where *I* is the amount of snowmelt infiltration, *S* is the degree of saturation as a decimal and *SWE* is the snowpack snow-water equivalent in mm. Degree of saturation was calculated using VWC data from the shallow (15 cm) sensors at the onset of snowmelt infiltration (i.e., the day the sensor responded to the snowmelt event). VWC values were divided by the saturation values for the respective sites (Appendix 1) to calculate degree of saturation.

Chapter 5: Results

Fall 2019

Fall precipitation in 2019 (October and November) totaled 170 mm, which was higher than the 30-year average of 121 mm and represented 20% of the annual sum of 850 mm (Figure 5.1a). A winter storm in late November quickly emplaced a 720 mm snowpack over a five-day period from November 27th to December 1st. The rapid development of snow cover prevented any deep soil frost from forming and allowed shallow soil temperatures at 15 cm depth to remain above freezing throughout the fall and into the winter (Figure 5.1b).

The shallow soil moisture sensor at the midslope site (15 cm depth) responded to every rain event larger than 5 mm throughout October and November (Figure 5.1c). Deeper soil moisture sensors (at 50 cm and 100 cm depth) at the midslope site showed a more limited response to rain events (Figure 5.1c). Both of the deeper sensors had higher volumetric water contents (VWC) than the shallow sensor throughout this period, and both sensors were close to saturation (Figure 5.1c; Appendix 1). VWC in the 100 cm sensor gradually declined throughout November (Figure 5.1c).

The hydraulic head in the midslope piezometer rose 113 cm during the first week of October in response to three discrete precipitation events totaling 88 mm (Figure 5.1d). The downslope piezometer also responded to the September 30th event (not shown) but had reached a local maximum by October 1st and showed a smaller (22 cm) response to the early October precipitation. The hydraulic gradient between the sites remained constant throughout the season (Figure 5.1d).

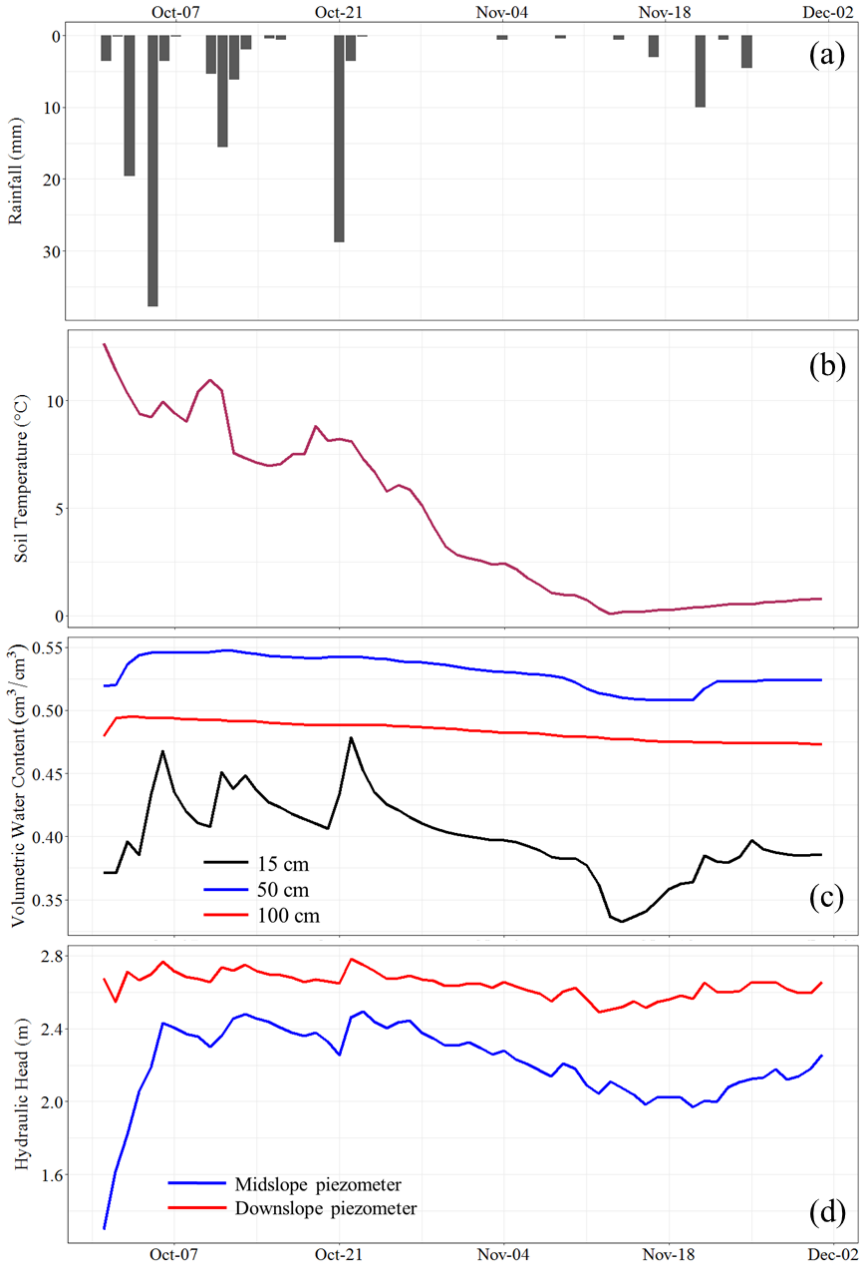

Figure 5.1: Daily data for (a) rainfall, (b) soil temperature at 15 cm depth and (c) VWC at the midslope site, and (d) total hydraulic head from October 1st to December 1st, 2019.

Winter 2019-2020

The winter 2020 snow season began on November 27th, 2019 and lasted until April 8th, 2020; Snow depth peaked at 711 mm on January 18th (National Weather Service). A rain/snow mix event occurred on December 29th and deposited 35.2 mm of rain and 152 mm of snow

(Figure 5.2a). The 15 cm sensor at the midslope site responded on the same day as the December 29th event and took roughly two weeks to return to pre-event conditions (Figure 5.2b). VWC in the deeper soil moisture sensors at 50 cm and 100 cm depth remained relatively constant throughout the winter (Figure 5.2b), and averaged 0.52 and 0.47 cm^3/cm^3, respectively (Dec 1st, 2019 to Mar 1st, 2020). Soil temperatures at 15 cm depth were consistently above 0°C throughout the winter, indicating no soil frost development (Figure 5.2c).

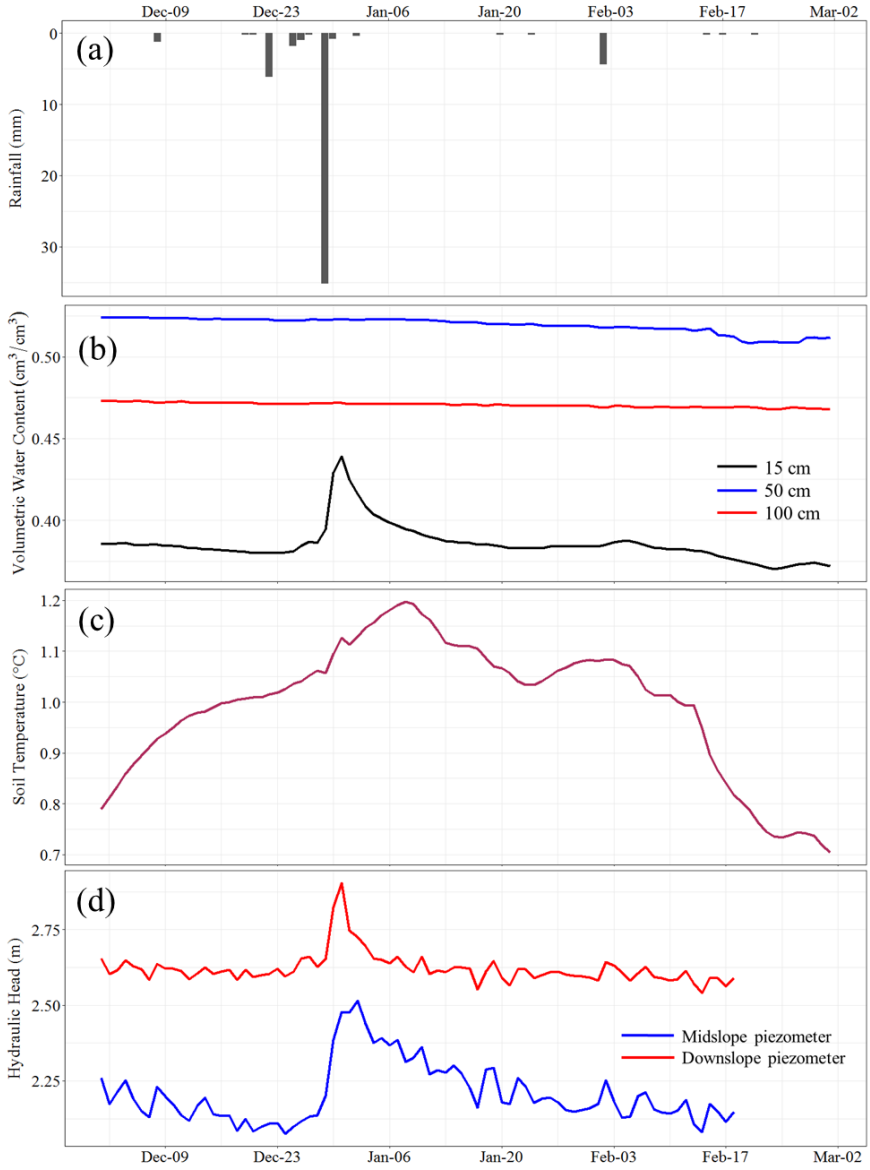

Figure 5.2: Daily data for (a) rainfall, (b) soil water content and (c) soil temperature at 15 cm depth at the midslope site, and (d) total hydraulic head from December 1st, 2019 to March 1st, 2020

Both the midslope and downslope piezometers responded to the December 29th event on December 30th (Figure 5.2d). The midslope and downslope piezometers rose 40 and 25 cm, respectively. The downslope piezometer returned to pre-event conditions after one week while the midslope piezometer returned to pre-event conditions after two weeks. Hydraulic head was consistently higher in the downslope piezometer than the midslope piezometer throughout the winter, indicating that flow continued to move laterally outward from the swale.

Spring 2020 (Snowmelt and Post-Melt Phase)

Water inputs from the release of snowpack snow-water equivalent (SWE) totaled 413 mm during the spring 2020 snowmelt period (Figure 5.3a). The onset of snowmelt occurred on March 17th, when SWE dropped by 67 mm over a two-day period. Peak melt rate occurred on March 21st, only four days after the onset of snowmelt, at a rate of 44 mm/day (Figure 5.3a). Only one rain event greater than 10 mm occurred during the snowmelt phase, a 34 mm event on March 29th. This event also deposited 99 mm of snowfall. Snowpack SWE continued to decrease until the snowpack was depleted on April 9th. Rainfall totaled 74 mm during the post-melt phase (April 9th to June 1st). Overall, spring rainfall (March, April, and May) totaled 121 mm, which was significantly less than the 30-year average of 187 mm (Figure 5.3a).

SWE data from the site were not available until March 11th, and snow depth data from the Duluth International Airport indicated that snowpack depletion began as early as March 6th. These early March melt events were likely small, evidenced by the small rises in water content at 15 cm and 50 cm depth (Figure 5.3b). In addition, air temperature data from the site indicated that temperatures dropped below freezing every night from March 6th to March 11th, which would have limited snowpack loss and led to only small melt events.

The 15 cm sensor initially responded to the onset of snowmelt on March 24th and reached its peak two weeks later on April 8th; VWC rose a total of 0.09 cm^3/cm^3 during this time (Figure

5.3b). VWC initially rose rapidly and then continued to rise gradually before it peaked at 0.495 cm^3/cm^3 (Figure 5.3b). The 15 cm sensor began to drain immediately following snowpack depletion, and VWC had nearly returned to pre-melt values before any measureable rise occurred at the deeper depths (Figure 5.3b). Neither of the deeper sensors (50 cm or 100 cm) showed any immediate response to snowmelt (Figure 5.3b). VWC in the 50 cm and 100 cm sensors continued to rise slightly through May, though it is unclear whether this rise was in response to late April and early May precipitation or a delayed response to snowmelt (Figure 5.3b).

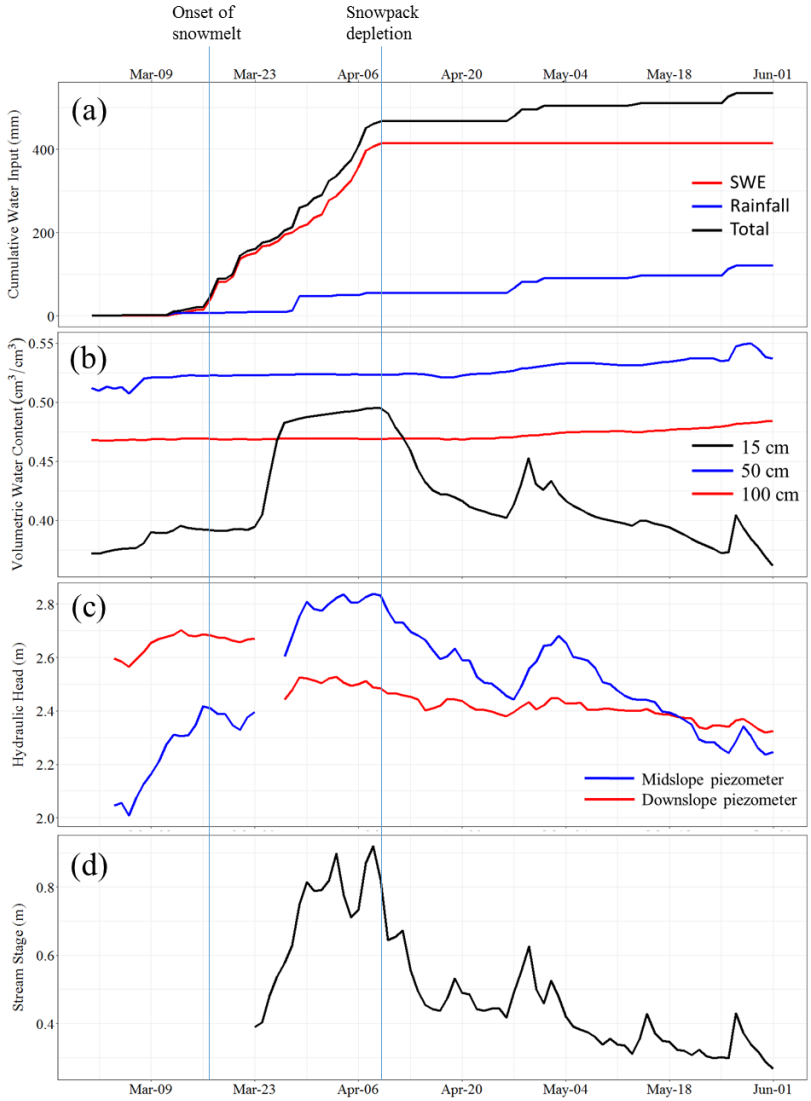

Figure 5.3: Daily data for (a) cumulative water input (SWE and rain), (b) VWC at the midslope site, (c) total hydraulic head, and (d) stream stage during the snowmelt and post-melt period from March 1st to June 1st, 2020.

Hydraulic head in both the midslope and the downslope piezometers began to rise on March 7th in response to the small melt events in early March (Figure 5.3c). Hydraulic head in the midslope piezometer began rising again on March 22nd, five days after the onset of snowmelt. Hydraulic head rose a total of 51 cm and peaked on April 8th (Figure 5.3c). Both piezometers were pumped dry on March 23rd while obtaining water samples; the piezometers took multiple days to recover fully. Thus, hydraulic head data from March 23rd to March 27th were removed from the dataset. The lack of water level rise in the downslope piezometer caused the hydraulic gradient between the midslope and downslope sites to reverse on March 27th, ten days after the onset of snowmelt (Figure 5.3c). The gradient did not reverse again until May 18th, almost two months after the onset of snowmelt.

The East Amity Creek stream gauge was reinstalled on March 23rd, 2020. Thus, no stream stage data were available prior to the onset of snowmelt. Stream stage in East Amity Creek reached a maximum of 92 cm on April 8th (Figure 5.3d). Stream stage began to decline immediately following snowpack depletion (Figure 5.3d).

Snowpack samples collected from March 4th to April 8th for stable isotope analysis had an average $\delta^{18}O$ of -16.0‰ (n = 21) (Figure 5.4a). Prior to the onset of snowmelt, $\delta^{18}O$ in both the swale and East Amity Creek resembled groundwater collected from the piezometers (around -12‰; Figure 5.4b; Figure 5.4c). On March 23rd, six days after the onset of snowmelt, $\delta^{18}O$ in the swale and East Amity Creek became increasingly depleted in response to snowmelt water entering the system (Figure 5.4b). Following snowpack depletion, $\delta^{18}O$ in both the swale and the East Amity gradually enriched until samples returned to pre-melt values in mid-May.

Water samples from the upslope and midslope lysimeters could only be obtained during periods of prolonged wet conditions. At the midslope site, the only period of prolonged wet conditions occurred during and following snowmelt. The midslope lysimeter showed a clear influence of snowmelt and had an average $\delta^{18}O$ of -14.3‰ (n = 33) (Figure 5.4c). In contrast, the

downslope lysimeter was relatively enriched throughout the snowmelt period with an average $\delta^{18}O$ of -9.24‰ (n = 50) (Figure 5.4c). Thus, the downslope lysimeter showed no influence of snowmelt during this period. Both the midslope and downslope lysimeters showed no visible isotopic response to the precipitation events in late April (Figure 5.4c).

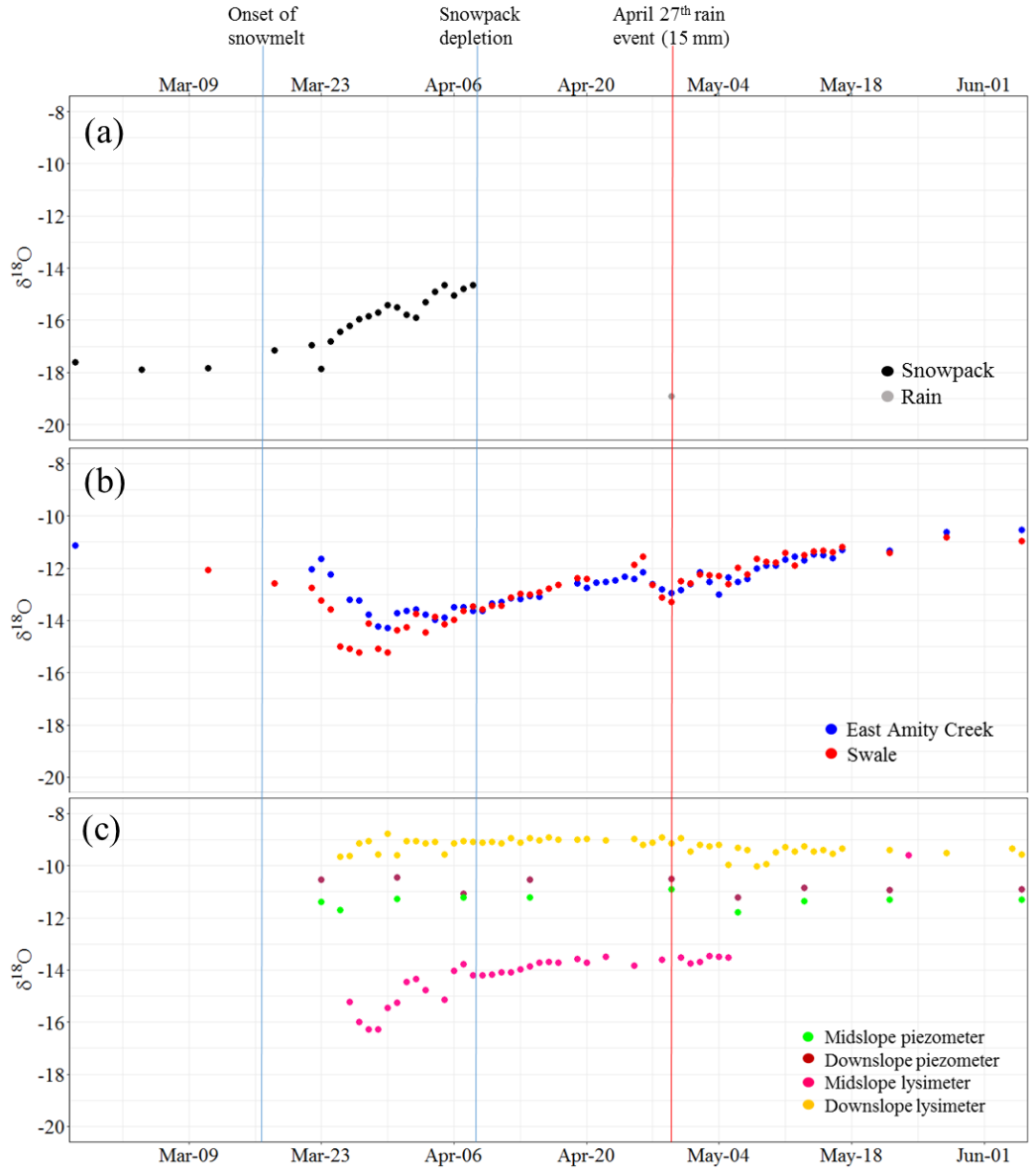

Figure 5.4: $\delta^{18}O$ values in (a) snow and rain, (b) the swale and East Amity Creek, and (c) piezometers and lysimeters during the snowmelt and post-melt period from March 1st to June 1st, 2020.

During the snowmelt and post-melt phase, the midslope and downslope piezometers had average $\delta^{18}O$ values of -11.3‰ (n = 9) and -10.8‰ (n = 8), respectively (Figure 5.4c). These values reflected average piezometer $\delta^{18}O$ for the full year, which were -11.2‰ (n = 19) and -10.7‰ (n = 18), respectively. Thus, despite the rise in hydraulic head, there was no clear isotopic influence of snowmelt at a depth of three meters at either site.

The influence of snowmelt within the swale and East Amity Creek is further highlighted by plotting the samples in dual-isotope space (Figure 5.5a). The difference in responses between the midslope and downslope sites is similarly apparent in dual-isotope space, with the downslope piezometer and lysimeter plotting entirely out of the range of snowpack values (Figure 5.5b).

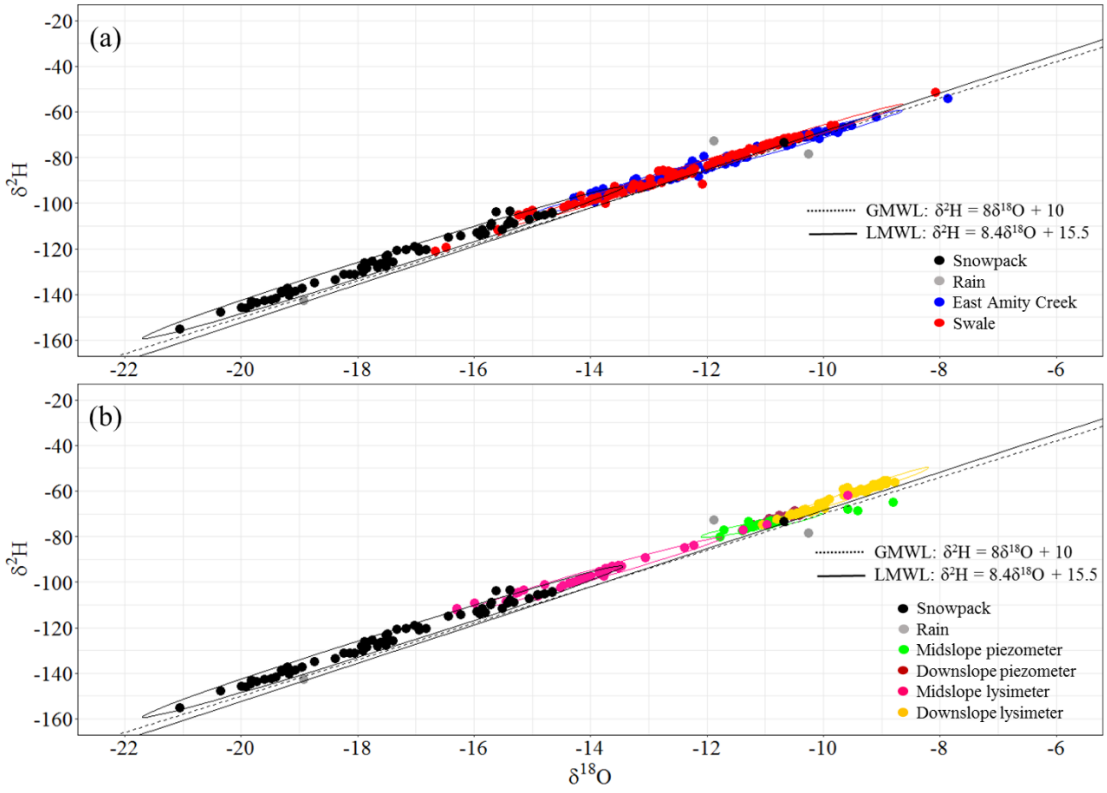

Figure 5.5: Dual-isotope plot showing the influence of snowmelt and rain on (a) surface water components and (b) shallow groundwater components. The data are plotted against the global meteoric water line obtained from Craig (1961) and the local meteoric water line obtained from Jasperson et al. (2018). Ellipses represent a multivariate t-distribution of the data.

Fall 2020

Rainfall in October and November of 2020 totaled 133 mm, which was higher than the 30-year average of 121 mm and represented 25% of the annual sum of 540 mm (Figure 5.6a). This annual sum was significantly lower than the 30-year average of 789 mm and approached the threshold for semi-arid conditions (Lane & Nichols, 1999).

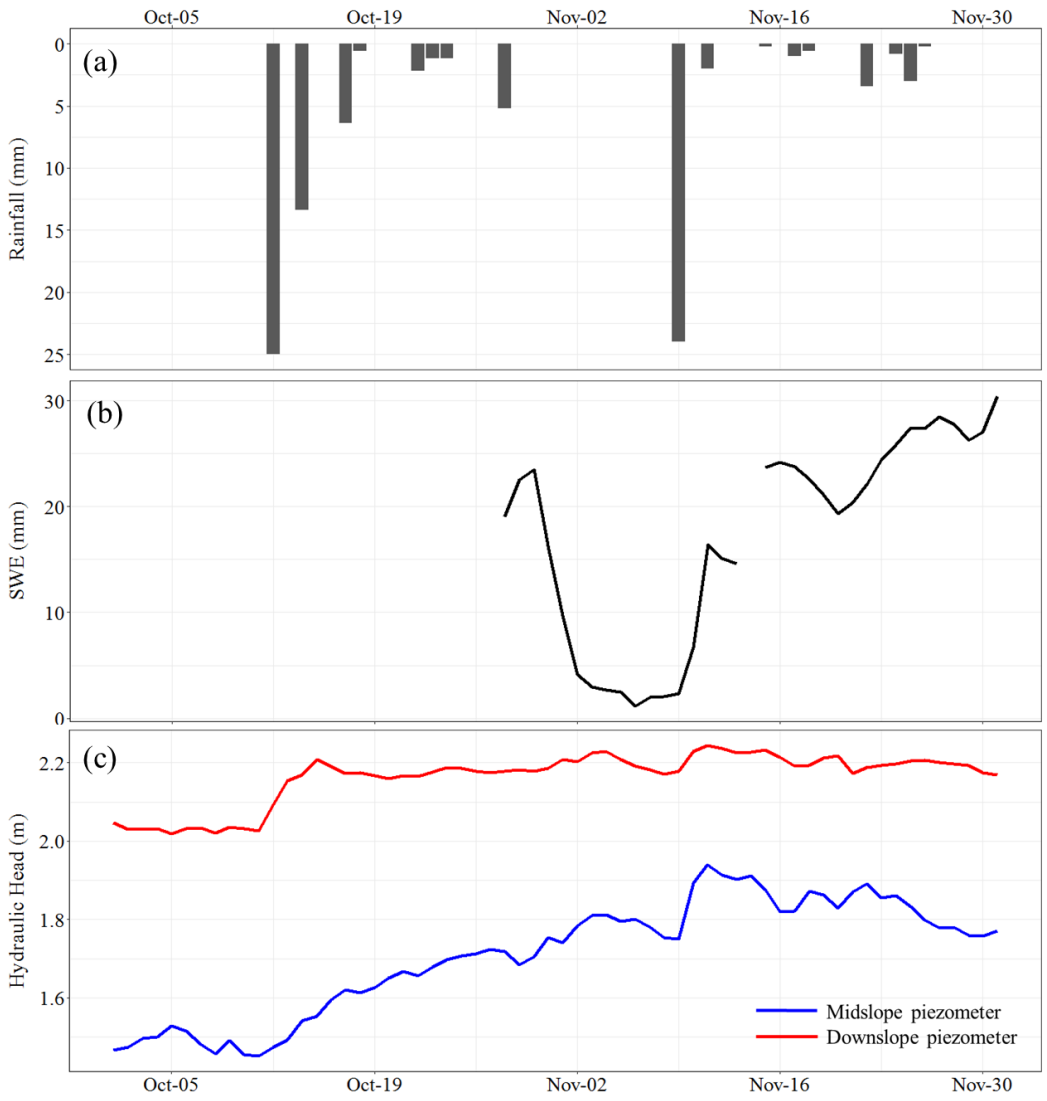

Figure 5.6: Daily data for (a) rainfall, (b) snow-water equivalent, and (c) total hydraulic head from October 1st to December 1st, 2020.

A snowfall event occurred on October 20th and deposited 140 mm of snow (Figure 5.6b). Snow-water equivalent (SWE) data were unavailable until October 28th. The snowpack began melting on October 30th, releasing 23.3 mm of SWE (Figure 5.6b). Sequential snowfall events in mid-November deposited a total of 279 mm of snow (Figure 5.6b). This snowpack remained throughout the rest of November and into the winter.

Hydraulic head in the midslope piezometer rose 5 cm on October 31st, in apparent response to the late October snowmelt event. The downslope piezometer, meanwhile did not respond to this event. Hydraulic head was consistently higher at the downslope site during the fall, and flow continued to move away from the swale throughout October and November (Figure 5.6c).

VWC and temperature patterns at the upslope and midslope sites were similar throughout fall 2020; however, VWC was consistently lower at all depths at the upslope site (Figure 5.7b). The shallow (15 cm) sensors at both the upslope and midslope sites responded to rain events larger than 10 mm and the snowmelt event at the end of October (Figure 5.7b). The 50 cm sensors at the upslope and midslope sites only responded to two events during this period: the snowmelt event at the end of October and a 24 mm rain event on November 9th (Figure 5.7b). The 100 cm sensors at both the upslope and midslope sites did not respond to any events during the fall period (Figure 5.7b). Soil temperatures at 15 cm depth never dropped below 2°C at either site; thus, soil frost was not present during the fall period (Figure 5.7c).

Snowpack samples collected during this period had an average $\delta^{18}O$ of -17.9‰ (n = 10) (Table 5.1). Rain samples collected from the October 12th and November 9th events had $\delta^{18}O$ values of -10.3‰ and -5.13‰, respectively. Lysimeter samples collected during the fall were limited to the shallow (15 cm) and deep (40 cm) lysimeters at the downslope site, as the soil was too dry to obtain a sample at any of the other sites. The swale, East Amity Creek, piezometers, and lysimeters showed no clear isotopic influence from the snowmelt event at the end of October

(Table 5.1). The lack of snowmelt influence in any part of the system was corroborated by plotting the samples in dual-isotope space (Figure 5.8).

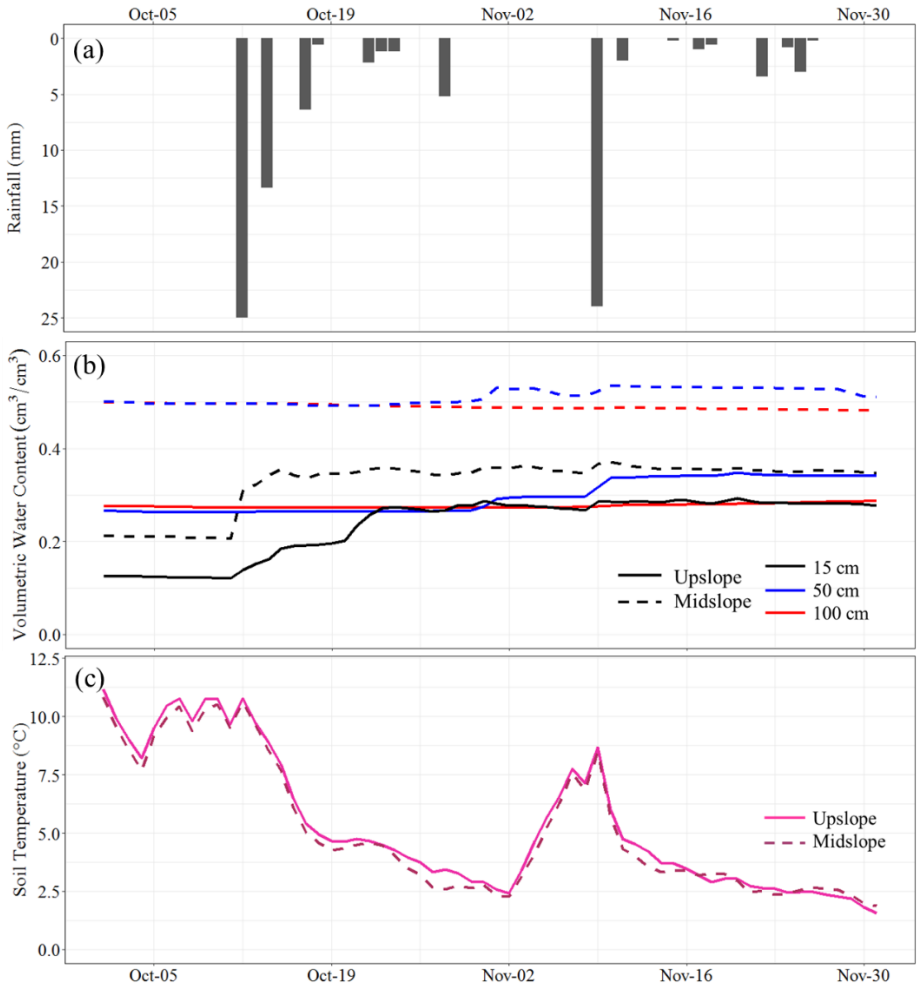

Figure 5.7: Daily data for (a) rainfall, (b) VWC, and (c) soil temperature at 15 cm depth at the upslope and midslope sites from October 1st to December 1st, 2020.

Table 5.1: Average $\delta^{18}O$ values from different sources during the fall 2020 period.

Sample	Average $\delta^{18}O$	# of samples (n)
Snowpack	-17.9‰	10
Swale	-10.7‰	10
East Amity Creek	-10.0‰	10
Downslope piezometer	-10.5‰	3
Downslope lysimeter (15 cm)	-9.88‰	4
Downslope lysimeter (40 cm)	-10.3‰	9
Midslope piezometer	-10.9‰	3

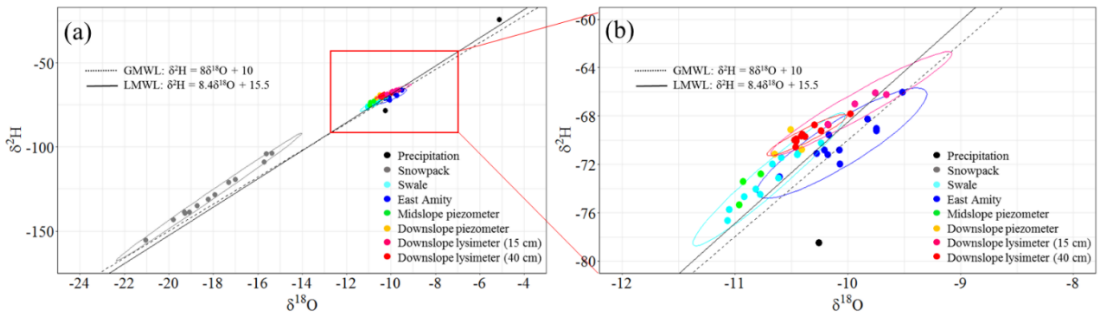

Figure 5.8: (a) dual-isotope plot for various sources of precipitation, surface water, and groundwater in the fall 2020 and (b) a zoomed-in plot highlighting the non-snow components of the system. Both figures are plotted against the global meteoric water line obtained from Craig (1961) and the local meteoric water line obtained from Jasperson et al. (2018). Ellipses represent a multivariate t-distribution of the data.

Winter 2020 – 2021

Snowpack depth during winter 2021 reached a maximum of 356 mm on February 21st (National Weather Service) while SWE reached a maximum of 152 mm on February 18th (Figure 5.9a). No rain events larger than 10 mm occurred during this period; the largest event was an 8.4 mm event on December 23rd, which was accompanied by 132 mm of snow.

The shallow (15 cm) sensors at the midslope and upslope sites fluctuated throughout this period despite no distinct snowmelt or rainfall events (Figure 5.9b). VWC in the 50 and 100 cm sensors at the upslope and midslope sites remained relatively constant during this period (Figure 5.9b). The 50 cm sensors at the upslope and downslope sites had average VWC values of 0.33 and 0.50 cm^3/cm^3, respectively, and the 100 cm sensors had average VWC values of 0.29 and 0.48 cm^3/cm^3, respectively. Soil temperatures at 15 cm depth never dropped below 0°C at the midslope site (Figure 5.9c). At the upslope site, soil temperatures at 15 cm depth dropped below 0°C on February 13th (Figure 5.9c). Soil temperature remained below 0°C throughout the rest of this period; thus, soil frost was likely present at the upslope site at the start of the snowmelt period.

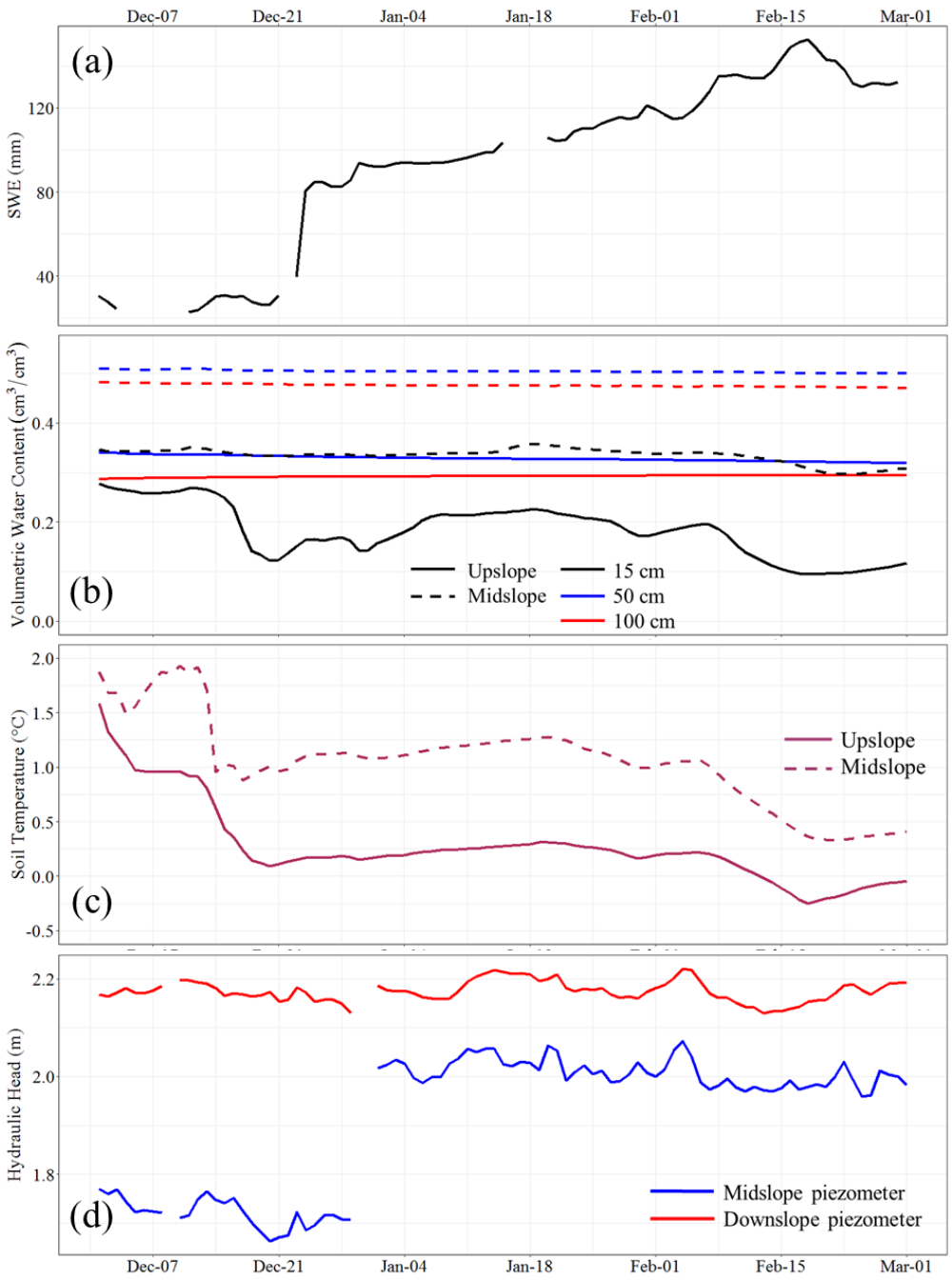

Figure 5.9: Daily data for (a) SWE, (b) VWC and (c) soil temperature at 15 cm depth from the midslope and upslope sites, and (d) total hydraulic head from December 1st, 2020 to March 1st, 2021.

Hydraulic head in the midslope and downslope piezometers remained relatively constant throughout this period (Figure 5.9d). A slug test was performed on December 29th to assess the

hydraulic properties of the till material. As a result, data from the following two days were removed. Hydraulic head was consistently higher in the downslope piezometer throughout the winter period; thus, flow continued to be moving outward laterally from the swale (i.e. a "losing" swale condition).

Spring 2021 (Snowmelt)

Snowmelt progression in spring 2021 largely occurred in two events: a small event that began on March 7th that released 27 mm of SWE and a larger event that began on March 17th that released a total of 103 mm of SWE over a five-day period (Figure 5.10a). Melt rate peaked at 46 mm/day on March 20th. The snowpack was primarily diminished by March 21st despite small patches of snow persisting in shaded areas. Thus, March 21st was considered the point of snowpack depletion. There was only one large rain event that occurred during this period, a 27 mm event that occurred on March 24th (Figure 5.10a). One snowfall event occurred after snowpack depletion, a 38 mm event on March 27th. This event also deposited 9 mm of rainfall.

Soil moisture sensors at both the upslope and downslope site responded to the March 7th snowmelt event on March 9th (Figure 5.10b). At the upslope site, VWC in the 15, 50, and 100 cm sensors rose in response to the snowmelt event (Figure 5.10b). At the midslope site, only the 15 and 50 cm sensors responded, and the 50 cm response was small (VWC rose only 0.02 cm^3/cm^3) (Figure 5.10b). The 15 cm sensors at the upslope and midslope sites responded to the March 17th snowmelt event on March 19th; neither of the deeper (50 and 100 cm) sensors at the upslope and midslope sites responded to this event (Figure 5.10b). The 15 cm sensor at the upslope site also responded to the rain event on March 24th; VWC rose 0.18 cm^3/cm^3 in a single day (Figure 5.10b).

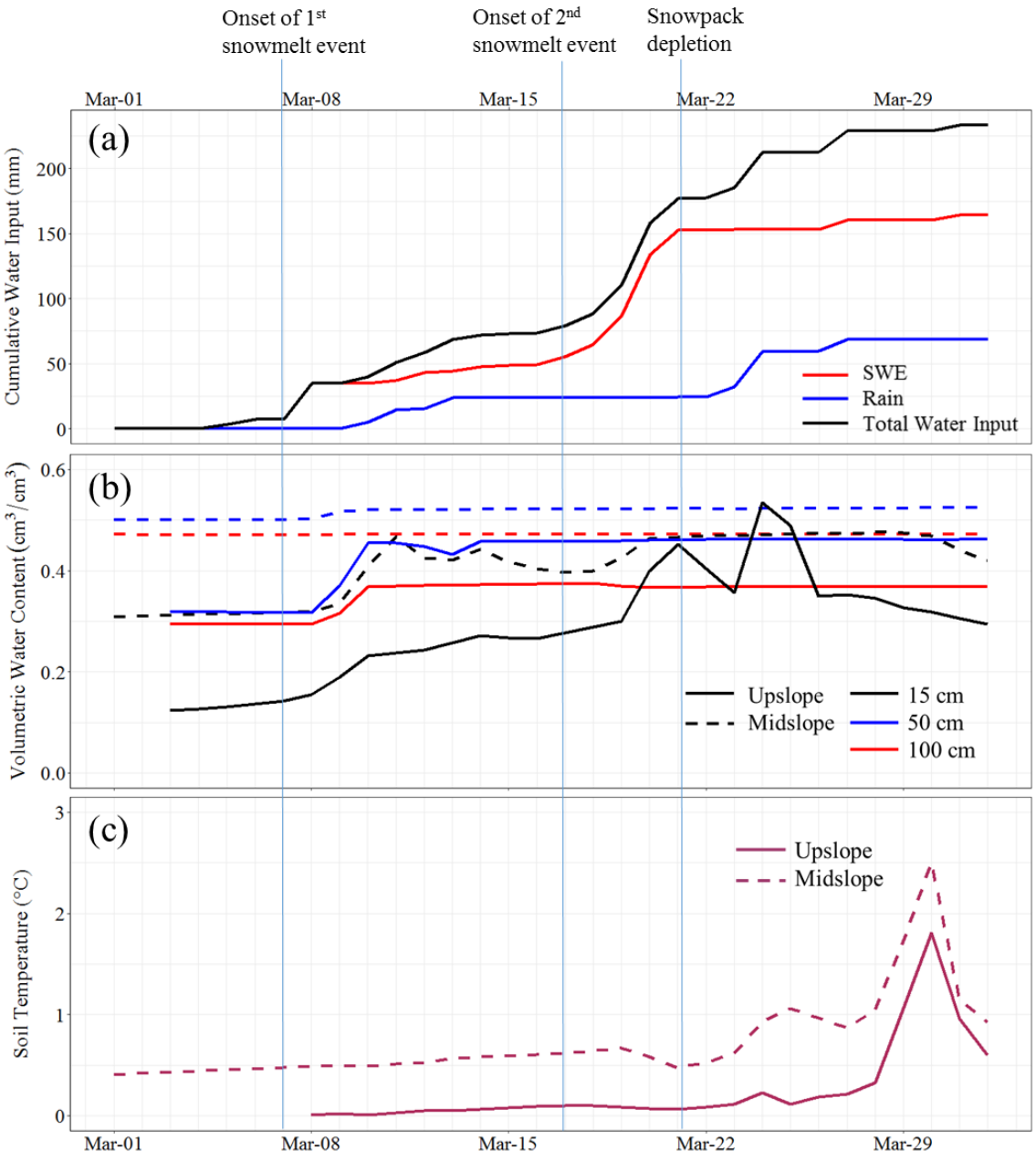

Figure 5.10: Daily data for (a) cumulative water input (SWE and rain), (b) VWC and (c) soil temperature at 15 cm depth at the midslope and upslope sites from March 1st, 2021 to April 1st, 2021.

Soil temperatures at 15 cm depth at the midslope site never dropped below 0.4°C during this period, indicating that soil frost was not present (Figure 5.10c). Soil temperatures at 15 cm depth at the upslope site did not rise above 0°C until March 8th (Figure 5.10c). Thus, there may

have been a significant amount of ice content in the surficial soil at the upslope site prior to the first snowmelt event.

The downslope and midslope piezometers responded to the first snowmelt event; the downslope piezometer responded on March 10th and the midslope piezometer responded on March 11th (Figure 5.11b). Water level in the downslope and midslope piezometers rose 18 cm and 41 cm, respectively, in response to this event. As a result, the hydraulic gradient between the two piezometers reversed on March 11th such that flow was moving from the midslope site to the downslope site (Figure 5.11b). The hydraulic gradient did not reverse again during the snowmelt period. The midslope piezometer also responded to the second snowmelt event on March 20th. The downslope piezometer did not respond to the second snowmelt event (Figure 5.11b).

Stream stage reached a local maximum of 45.3 cm on March 14th following the first snowmelt event and small rain events on March 11th and March 13th (Figure 5.11c). Stream stage reached another local maximum on March 22nd following the second snowmelt event and peaked at 96.3 cm on March 24th following a 27 mm rain event (Figure 5.11c).

Snow samples collected during this time period had an average $\delta^{18}O$ value of -19.0‰ (n = 16) (Table 5.2). The swale, East Amity Creek, and the midslope and upslope lysimeters showed the strongest influence of snowmelt (Table 5.2). Sampling of the midslope and downslope piezometers was too limited during the snowmelt period and thus no response to snowmelt could be discerned from the isotope samples (Table 5.2). The $\delta^{18}O$ values in the downslope and midslope piezometers reflected the yearly average values of -10.7‰ (n = 23) and -10.9‰ (n = 24), respectively.

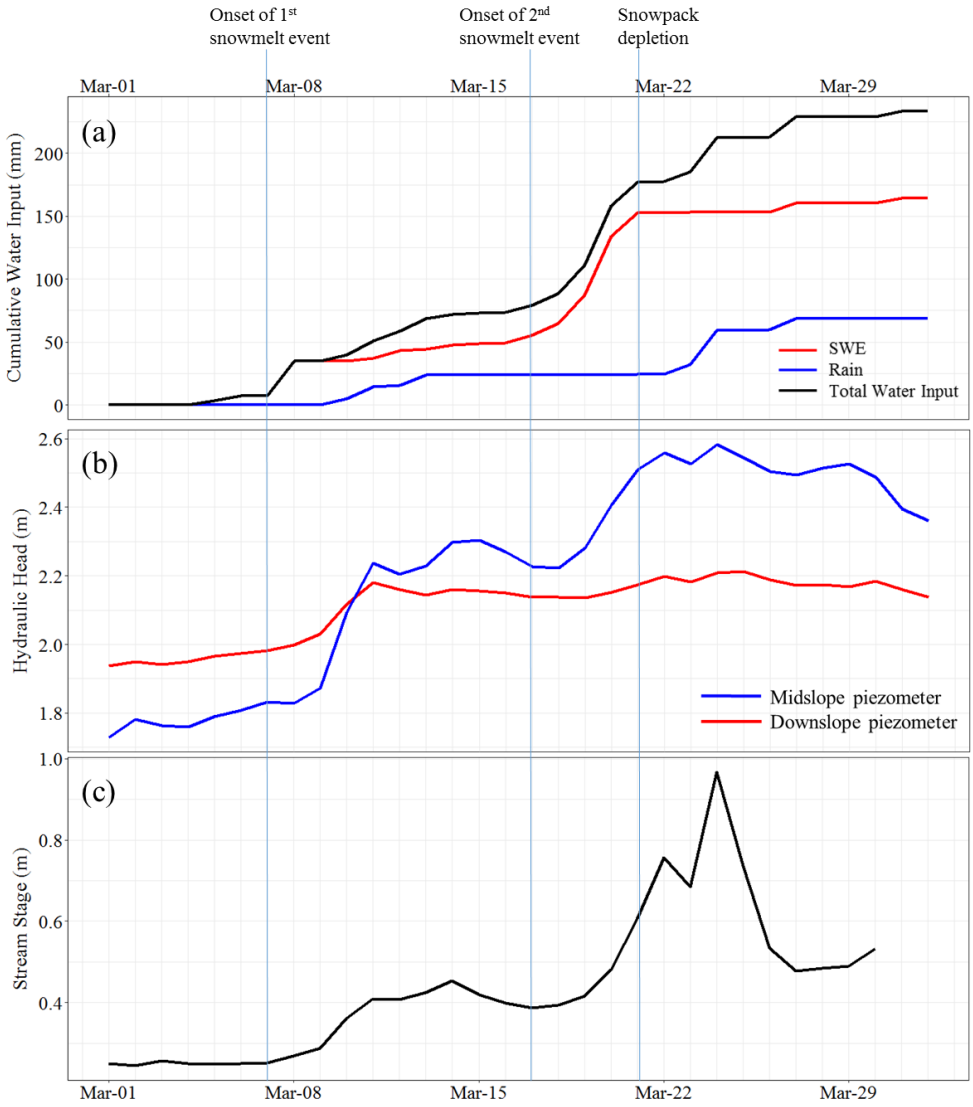

Figure 5.11: Daily data for (a) cumulative water input (SWE and rain), (b) total hydraulic head, and (c) stream stage from March 1st, 2021 to April 1st, 2021.

Table 5.2: Average $\delta^{18}O$ values from different sources during the snowmelt 2021 period.

Sample	Average $\delta^{18}O$ value	# of samples (n)
Snow	-19.0‰	16
Swale	-13.7‰	21
East Amity Creek	-12.4‰	22
Downslope piezometer	-10.5‰	2
Downslope lysimeter (15 cm)	-10.8‰	11
Downslope lysimeter (40 cm)	-10.6‰	6
Midslope piezometer	-10.2‰	2
Midslope lysimeter (15 cm)	-14.0‰	5
Midslope lysimeter (40 cm)	-13.1‰	8
Upslope lysimeter (40 cm)	-12.0‰	7

The precipitation events on March 24th and March 27th had average $\delta^{18}O$ values of –11.9‰ and –19.0‰, respectively (Figure 5.12a). The $\delta^{18}O$ values in the swale and East Amity Creek became increasingly depleted following the onset of the first snowmelt event; values in the swale became depleted one day prior to those in East Amity Creek (Figure 5.12b). The swale and East Amity Creek reached minimum $\delta^{18}O$ values of -16.7‰ and -13.9‰, respectively, on March 10th. Values in the swale and East Amity Creek enriched after the initial snowmelt period and dropped only slightly in response to the second snowmelt event (Figure 5.12b). The deeper 40 cm lysimeter at the midslope site displayed a notable drop in $\delta^{18}O$ following the second snowmelt event (Figure 5.12c).

The influence of snowmelt on surface water components (the swale and East Amity Creek) and the midslope site is shown clearly when plotting the samples in dual-isotope space (Figure 5.13). The swale displayed a stronger influence of snowmelt than East Amity Creek (Figure 5.13a). The lysimeters from the downslope sites showed little or no influence of snowmelt (Figure 5.13b). Samples from the upslope lysimeter (40 cm) plotted in between the midslope and downslope lysimeters both in time-series data and in dual-isotope space (Figure 5.12c; Figure 5.13b). This finding contradicted VWC data from the upslope site, which showed that snowmelt infiltration occurred to a depth of 100 cm during the first snowmelt event. However, lysimeter samples from the upslope site were not obtained until after the onset of the second snowmelt event, in which the deeper sensors at the upslope site did not respond. As a result, $\delta^{18}O$ in the upslope lysimeter likely reflected an intermediate influence of snowmelt relative to the midslope and downslope sites.

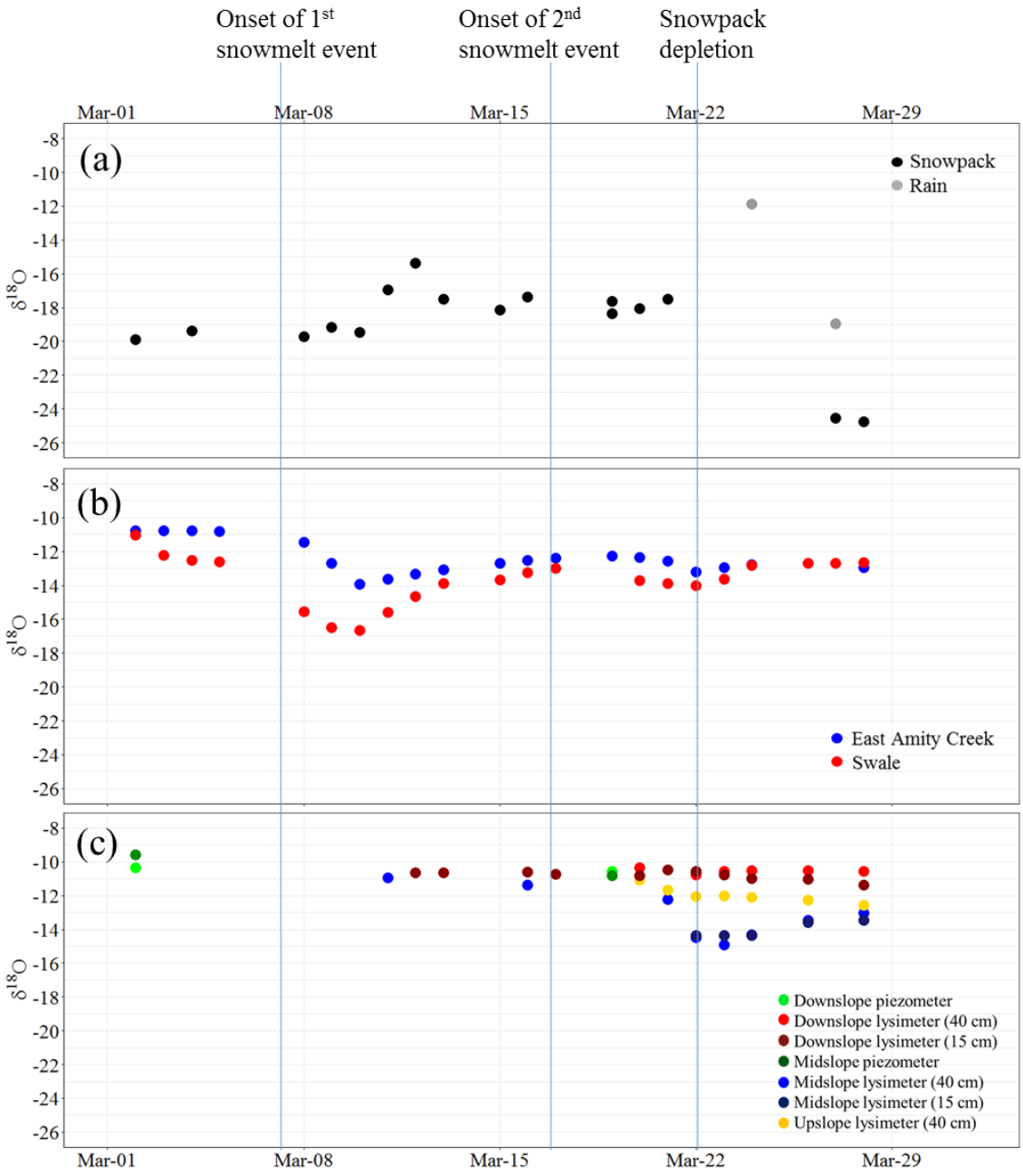

Figure 5.12: $\delta^{18}O$ values in (a) snow and rain, (b) the swale and East Amity, and (c) piezometers and lysimeters during the snowmelt period from March 1st to April 1st, 2021.

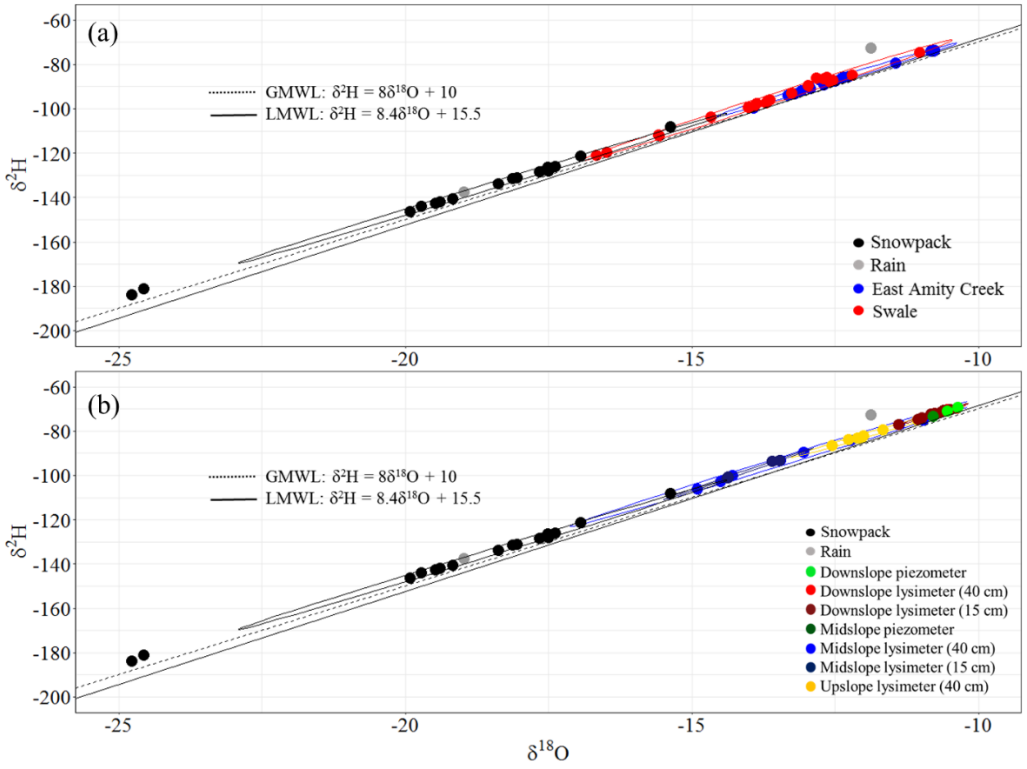

Figure 5.13: Dual-isotope plot showing the influence of snowmelt on (a) surface water components and (b) groundwater components. Both figures are plotted against the global meteoric water line obtained from Craig (1961) and the local meteoric water line obtained from Jasperson et al., 2018. Ellipses represent a multivariate t-distribution of the data.

Estimating Snowmelt Infiltration

Equation 4.6 was applied to VWC data from the midslope site in 2020 and applied to VWC data from the midslope and upslope sites for both snowmelt events in 2021 (Table 5.3).

Table 5.3: Estimation of snowmelt infiltration based on empirical equation from Gray and Landine (1985).

Snowmelt season	**Site**	**S**	**SWE (mm)**	**I (mm)**	**% Infiltration**
2020	Midslope	0.80	413	33.7	8.2%
2021 (1st snowmelt event)	Midslope	0.67	27	11.3	42%
2021 (2nd snowmelt event)	Midslope	0.86	103	10.5	10%
2021 (1st snowmelt event)	Upslope	0.35	27	22.3	83%
2021 (2nd snowmelt event)	Upslope	0.75	103	18.7	18%

At the midslope site, the overall amount of infiltration was greater during the 2020 snowmelt season but the fraction of snowmelt that infiltrated was greater during the 2021

snowmelt season (Table 5.3). For both snowmelt events in 2021, the upslope site had a larger estimated amount of overall snowmelt infiltration relative to the midslope site (Table 5.3). Percent infiltration was greater for the first snowmelt event at both the upslope and midslope sites (Table 5.3).

Chapter 6: Conceptual Model

A conceptual model was developed for the site to explain the timing and mechanisms of shallow groundwater movement in response to rainfall and snowmelt events. The model generally follows the depression-focused model of groundwater recharge but includes the influence of tile drainage as well (see Chapter 3). This conceptual model was based on preliminary soil moisture and groundwater data obtained during the first year of study (2019) and visual observations of surface water drainage during snowmelt. Data from the second year of study (2020) was used to support the conceptual model and identify missing components or inaccurate assumptions.

One of the key assumptions the model makes is that the piezometers at the downslope and midslope site are installed within the water-table mound surrounding the swale. Thus, they should be in good hydrologic contact with the depression at the bottom of the hillslope transect. The downslope site, being in closer proximity to the swale, should thus experience a stronger influence from the tile drainage. The midslope site would also presumably be influenced by the drain tile but to a lesser extent. The upslope site, at a sufficient distance from the swale, should not be influenced by the drain tiles. This could explain why the upslope piezometer remained dry throughout the duration of the study.

Another key assumption that the model makes is that the infiltration capacity and hydraulic conductivity of the soil are significantly higher at the soil surface relative to the deeper soil. This allows for significant infiltration to occur during rainfall or snowmelt events, but this infiltration is limited to the upper 50 cm of soil. The infiltration capacity of the soil also decreases with increasing saturation such that significant infiltration is only possible during the early stages of a rainfall or snowmelt event. The piezometers should not be in good contact with the surficial soil layer and piezometer responses should be more related to the response of the depression. The

piezometers should behave as though they are in a saturated, semi-confined aquifer due to the low permeability of the overlying material.

6.1) System Response to Rainfall

Prior to rainfall events, the system is presumably dry and the water level in the depression at the bottom of the hillslope is relatively low (Figure 6.1a). As precipitation begins, the high permeability of the near-surface soil allows most of this precipitation to infiltrate. The infiltration capacity begins to decrease as more pores become filled with water; at a certain point, the rate of precipitation exceeds the infiltration rate in the soil and surface runoff (overland flow) is generated. The surface runoff is routed to the swale and the depression at the base of the hillslope begins to fill with water. The reduced infiltration capacity of the soil at depth promotes lateral subsurface flow that is also routed to the depression (Figure 6.1b). The rise in hydraulic head in the swale causes a pressure-front pulse displacement (PFPD) wave to be propagated outward from the swale, which in turn triggers a groundwater displacement (GD) wave to be propagated in the same direction. The PFPD wave is a result of aquifer compressibility whereas the GD wave results from the gravitational drainage of pore spaces. The PFPD wave moves significantly faster than the GD wave and can be detected by the pressure transducers in the piezometers. As a result, the piezometers start to respond to the rainfall relatively quickly; the time-lag between the onset of precipitation and the onset of response is limited by the infiltration capacity of the soil during the early stages of the rainfall event. Following the onset of piezometer response, water levels in the piezometers rise slowly over the next couple days as the GD wave slowly moves groundwater away from the depression.

The model suggests that the piezometers would not respond to small precipitation events because it is less likely that the infiltration capacity of the soil would be exceeded. By extension, the model also suggests that the piezometers would show a larger response to subsequent rainfall events, even if they are relatively small, due to the reduced infiltration capacity of the soil.

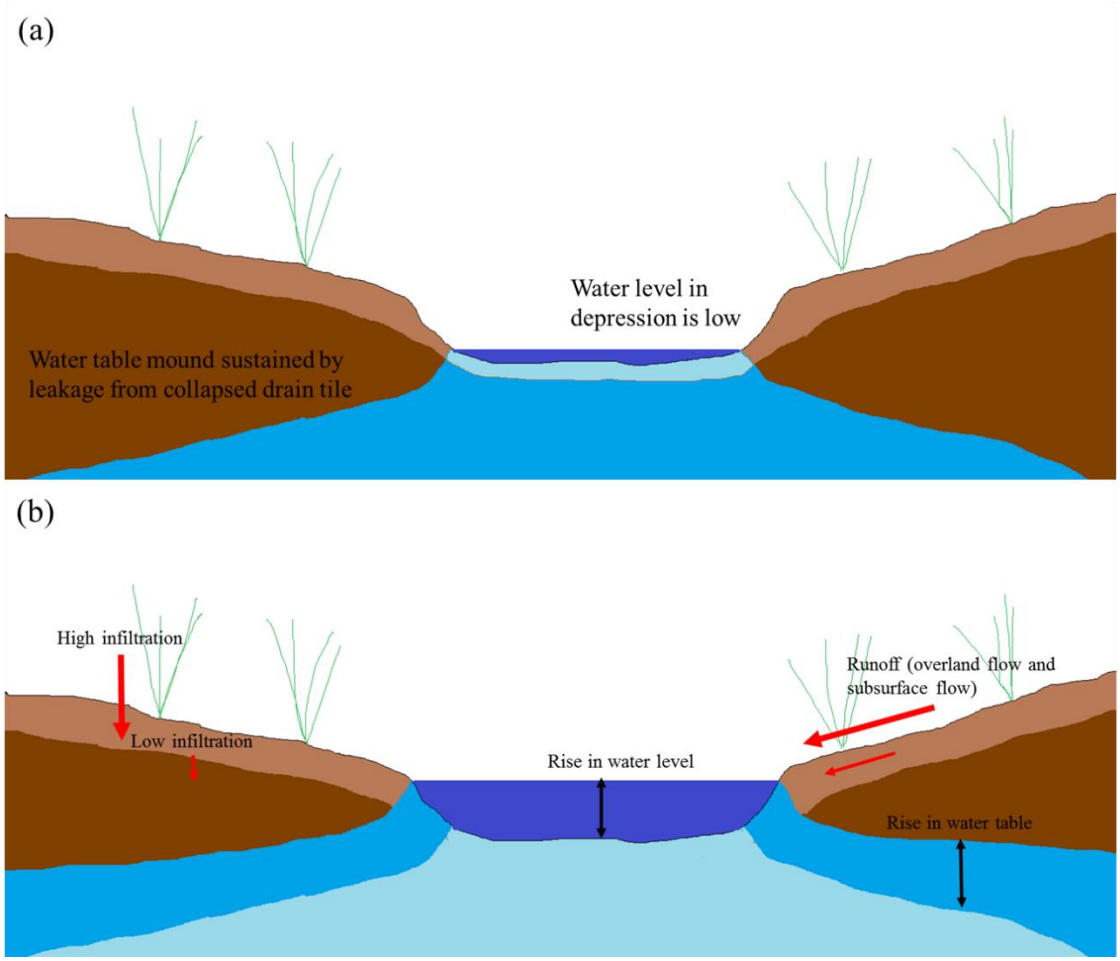

Figure 6.1: Diagram illustrating the system (a) prior to rainfall and (b) in response to rainfall. Lighter colored soils indicate the enhanced infiltration capacity near the surface.

6.2) System Response to Snowmelt

The system response to snowmelt is dependent on the presence of soil frost and the size of the snowpack. I present two conceptual models: one for a spring with a smaller snowpack and a deeper soil frost, i.e. an "open" winter, and one for a spring with a larger snowpack and no soil frost.

Groundwater response to a thin snowpack with deeper soil frost

Prior to the onset of snowmelt, the soil at each hillslope site is presumably frozen to a shallow depth. The soil beneath the swale, however, is not frozen due to the constant input of relatively warm (~7°C) discharge from the collapsed tile (see Chapter 3). As snowmelt begins, a large portion of snowpack snow-water equivalent (SWE) is lost to surface runoff due to the reduced infiltration capacity of the frozen soil. This surface runoff is routed to the depression at the base of the hillslope where it begins to pond. The ponding water causes a change in hydraulic head within the depression, which transmits a PFPD wave laterally (similar to the rainfall response). As a result, the piezometers would show a response earlier than the soil moisture sensors. The soil moisture sensors would not show a significant response until the ground had sufficiently thawed, at which point there may only be a small amount of SWE available for infiltration. Infiltration would occur rather quickly at shallow depths but would still be limited for deeper depths. Once the infiltration capacity of the soil is exceeded, the rest of the SWE would mostly be lost to surface runoff. The lower overall amount of SWE means that surface runoff would likely not exceed the storage capacity within the depression and thus a fill-and-spill network would not develop (see *Groundwater dynamics in formerly glaciated systems* section in Chapter 2). The lower volume of SWE would also limit the water level rise in each piezometer, and flow would continue to be away from the swale throughout this period, i.e. a losing-swale scenario.

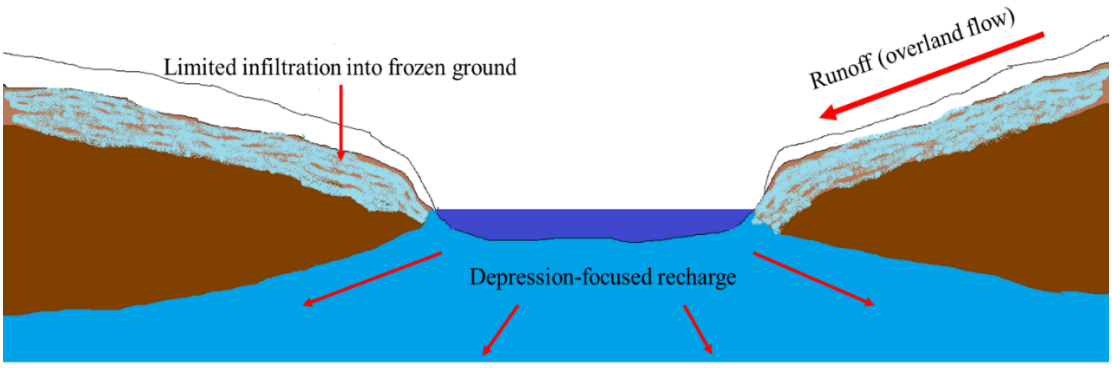

Figure 6.2: System response to snowmelt for a year with a small snowpack and soil frost.

In this conceptual model, the presence of the drain tile influences groundwater response by preventing soil frost from forming underneath the pond, which allows depression-focused recharge to reach the piezometers earlier in the snowmelt period. It also maintains the water table mound underneath the depression throughout the winter, which would cause the soils at the downslope and midslope site to be relatively wet prior to freezing. The wetter frozen soil promotes more surface runoff generation early during the snowmelt period, which also accelerates the piezometer response.

Groundwater response to a thick snowpack with no soil frost

Prior to the onset of snowmelt, the soil at each hillslope site would have the potential to infiltrate meltwater almost immediately after the onset of snowmelt. However, the larger volume of SWE would cause the infiltration capacity of the soil to be exceeded relatively quickly, causing surface runoff generation soon after the onset of infiltration. The surface runoff would pond in the depression and cause a PFPD wave that is routed to the piezometers; as a result, the piezometer response should lag slightly behind the soil moisture response. The large amounts of surface runoff generated are enough to exceed the depression storage within the swale; as a result, a fill-and-spill network is developed within the swale that connects numerous depressions that were previously isolated. This network drains to the South towards East Amity Creek, moving large

amounts of meltwater away from the site. This limits the overall amount of water available for depression-focused recharge. The fill-and-spill network would also limit the piezometer response since it is dependent on a change in hydraulic head within the depression; once depression storage is exceeded, the hydraulic head in the depression would become relatively constant and would not trigger a large PFPD. Thus, piezometer response at the downslope and midslope site should be limited to the early stages of snowmelt before depression storage is exceeded. There would not be enough water level rise in the midslope piezometer to shift the direction of groundwater movement and thus the depression would continue to act as a "losing" water body throughout the year.

The influence of the drain tile is less pronounced in this conceptual model. Leakage from the drain tile keeps the water level in the depression relatively high prior to snowmelt, which causes depression storage to be exceeded earlier in the snowmelt period. However, the larger overall volume of SWE in this model would likely exceed the depression storage regardless of what the initial water level in the depression is. Thus, it may cause the piezometer response to cease earlier in the snowmelt period, but the overall volume of depression-focused recharge would be similar even in the absence of the drain tile.

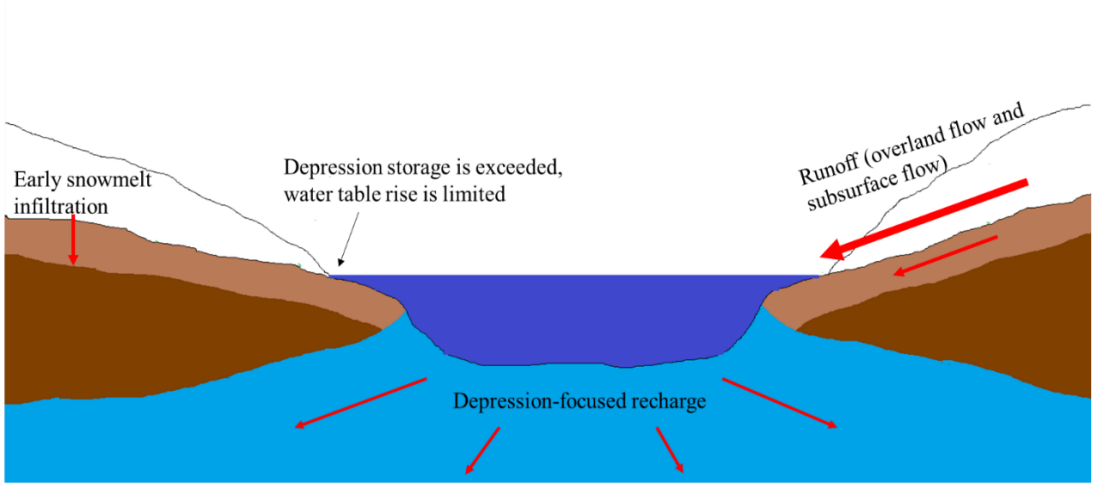

Figure 6.3: System response to snowmelt in a year with a large snowpack and no soil frost.

Chapter 7: Discussion

The results of this study provide insight on the fate and transport of rainfall and snowmelt in formerly glaciated regions. Soil moisture responses, piezometer responses, and snowmelt partitioning were examined for two study years with differing amounts of snowpack SWE. The conceptual model presented in Chapter 6 describes shallow groundwater movement at the site following rainfall and snowmelt events, with a focus on depression-focused recharge and lateral subsurface flow. Additionally, the model examines the role of soil frost in partitioning snowmelt and the influence of tile drainage on the timing and magnitude of shallow groundwater recharge.

7.1) Soil Moisture Responses to Precipitation and Snowmelt

Shallow (15 cm) soil moisture sensors at both the upslope and midslope sites responded to rainfall and snowmelt events throughout the fall and spring of each study year. The largest responses in shallow soil moisture were observed during early fall precipitation (Figure 5.1b; Figure 5.6a) and during snowmelt (Figure 5.3b; Figure 5.11b). In contrast, deeper (50 and 100 cm) soil moisture responses to rainfall and snowmelt were limited to only a few events at both the upslope and midslope sites throughout the two study years. The lack of responses at deeper depths was observed even at the 10-minute intervals at which the sensors collected data. The relative frequency of responses in the 15 cm sensors compared to the 50 and 100 cm sensors illustrates the enhanced permeability of the surficial soil relative to the deeper soils. This enhanced permeability was consistent with the soil texture from 0 to 30 cm, which was slightly sandier (Appendix 1). The presence of a more-permeable layer overlying a less-permeable layer supports the notion that lateral subsurface flow occurs following snowmelt events (Weiler et al., 2006; Chifflard et al., 2019; Mohammed et al., 2019). This notion is illustrated in snowmelt data from both study years. Shallow soil moisture sensors drained rapidly following snowpack depletion despite no apparent rise in VWC at deeper depths, which suggests that deeper

percolation was limited (Figure 5.3b; Figure 5.10b). Thus, infiltrating water was likely deflected laterally. Other groundwater studies in glacial tills have found that lateral subsurface flow can be a significant redistribution mechanism following snowmelt (Stumpp & Hendry, 2012; Jones & Tomasek, 2015; Pam et al., 2020).

However, the lack of response in the deeper soil moisture sensors does not necessarily mean that percolation did not occur. At the midslope site, VWC in the 50 and 100 cm sensors receded throughout the fall (Figure 5.1b) and winter (Figure 5.2a; Figure 5.9b), but remained fairly constant during the snowmelt periods (Figure 5.3b; Figure 5.11b). Thus, percolation was likely occurring at deeper depths during snowmelt periods at a rate that balanced the draining of the soil. There is evidence of snowmelt percolation occurring to a depth of 40 cm; water samples collected from lysimeters at 40 cm depth at the upslope and midslope sites showed an isotopic influence of snowmelt (Figure 5.5b; Figure 5.13b). However, the 40 cm lysimeter at the downslope site showed no influence of snowmelt during snowmelt periods (Figure 5.5b; Figure 5.13b). Thus, percolation to deeper depths did occur, but it was spatially limited to the midslope and upslope sites and was likely a small portion of the overall amount of water that infiltrated the soil surface.

The influence of soil frost on the timing of soil moisture response to snowmelt was hard to determine, as soil frost was minimal (as determined by soil temperature) during both study years. Despite the overall lack of soil frost, there were delays between the onset of snowmelt and an increase in shallow soil moisture during both years (Figure 5.3b; Figure 5.11b). At the midslope site, this delay was seven days long in 2020 and two days long in 2021. Several studies documented soil frost delaying soil moisture response to snowmelt infiltration (Daniel & Staricka, 2000; Iwata et al., 2011; Harpold et al., 2014). Of these, only Daniel & Staricka (2000) examined soil moisture response in glacial tills; they found that the timing of soil moisture response to snowmelt infiltration correlated to the thawing of a thin frost layer near the soil

surface. Soil temperature data at 15 cm depth indicated that soil frost was not present in the 2020 snowmelt season and was limited to the upslope site in the 2021 snowmelt season. Thus, the presence of frost within the soil column cannot fully explain the delay between the onset of snowmelt and the increase in shallow soil moisture during both study years.

One possible explanation for the delayed soil moisture response to snowmelt infiltration may be the presence of ice lenses at the base of the snowpack that restrict early infiltration (Kane & Stein, 1983; Iwata et al., 2011). Ice lenses typically delay infiltration by one or two days, though they can delay infiltration by as much as two months (Iwata et al., 2011; Pavlovskii et al., 2019). Ice lenses are more likely to form in soils that are wet prior to freezing (Kane & Stein, 1983). Given that fall 2019 was wetter than fall 2020, this could explain why the delay was greater for the 2020 snowmelt season. The propensity of ice lenses to form from midwinter rain or early melt events suggests that the winter 2019-2020 rain event could have also had an influence on the greater delay during the 2020 snowmelt season (Mohammed et al., 2019; Pittman et al., 2019; Pavlovskii et al., 2019).

7.2) Shallow Groundwater Responses to Precipitation and Snowmelt

Between fall 2019 and spring 2021, the midslope and downslope piezometers responded frequently to precipitation events despite the low hydraulic conductivity of the soils at depth (10^{-8} m/s). These responses supported the proposed conceptual model and other findings that depression-focused recharge allows for greater communication between precipitation events and shallow groundwater (Chapter 5; Jones & Tomasek, 2015; Hayashi et al., 2016). The piezometers displayed relatively rapid initial responses to precipitation despite their low hydraulic conductivity (10^{-8} m/s), and often responded on the same day as rainfall events (Figure 5.1d); they subsequently took several days to peak following an event. This illustrated the difference between a pressure-front pulse displacement (PFPD) wave and a groundwater displacement (GD) wave under saturated conditions (Chesnaux, 2018). Saturated conditions were presumably maintained

by a water table mound formed by the swale that was in contact with the piezometers. A PFPD wave can be much faster than a GD wave because it is dependent on the diffusivity of the saturated soil rather than the effective porosity of the soil (Chesnaux, 2018). Thus, the piezometers essentially behaved as though they were in a confined system and mostly out of contact with the surficial soils. As a result, the initial change in hydraulic head in the depression following a precipitation event was propagated to piezometers relatively quickly, while actual groundwater movement to the piezometers occurred more slowly over the following days.

Piezometer response to snowmelt was mostly limited to the midslope site (Figure 5.3c; Figure 5.5c; Figure 5.12b), as the downslope lysimeters showed little to no influence of snowmelt during either study year (Figure 5.4c; Figure 5.6; Figure 5.13c). The lack of response in the downslope piezometer was hard to explain under the current conceptual model, as the swale runoff generated from the snowmelt should have caused a signal to be propagated to the downslope piezometer (see Chapter 5). Since the midslope piezometer did respond to snowmelt, any up-slope propagation of a snowmelt signal would also be detected in the downslope piezometer. The reversal of the hydraulic gradient toward the swale during the snowmelt period represents a further breakdown in the depression-focused recharge theory and cannot explain the hillslope response to snowmelt.

However, for hillslopes in temperate regions that experience snow, hydrologic connectivity across the hillslope may be limited to wetter periods throughout the year, such as snowmelt periods (McNamara et al., 2005). At this particular field site, it is possible that the unsaturated zone at the midslope and upslope site were not hydrologically connected to the downslope swale system for most of the year. Thus, for most of the year, the depression-focused recharge model explained hydrologic responses to water inputs in the midslope piezometer. During the snowmelt and post-melt phase, however, the unsaturated zones at the midslope and upslope sites were sufficiently wetted such that the entire hillslope became connected, and lateral subsurface flow

from the upslope site could lead to a response in the midslope piezometer. The lack of clear isotopic influence in the midslope piezometer following snowmelt (Figure 5.4c; Figure 5.13c) could support this notion; isotopic signals can be lost as water is transmitted via lateral subsurface flow due to the enhanced mixing with residual pore waters (Stumpp & Hendry, 2012; Mueller et al., 2014; Pavlovskii et al., 2018). The lack of isotopic signal could also be due to the fact that samples were collected infrequently and that the piezometers were not purged prior to sampling. Both of these conditions could cause an attenuated snowmelt signal.

The hillslope connectivity model also cannot explain the lack of response in the downslope piezometer. One explanation consistent with the depression-focused recharge model considers that, in order for a signal to propagate outward from the swale, there must be an observed change in hydraulic head within the swale. During snowmelt periods, substantial runoff can exceed the depression storage capacity of the swale such that any additional water input does not significantly raise the hydraulic head within the swale (Figure 7.2). Assuming the water level in the swale was relatively high prior to snowmelt, a significant change in head might not have occurred and thus a snowmelt signal would not have been observed in the downslope piezometer.

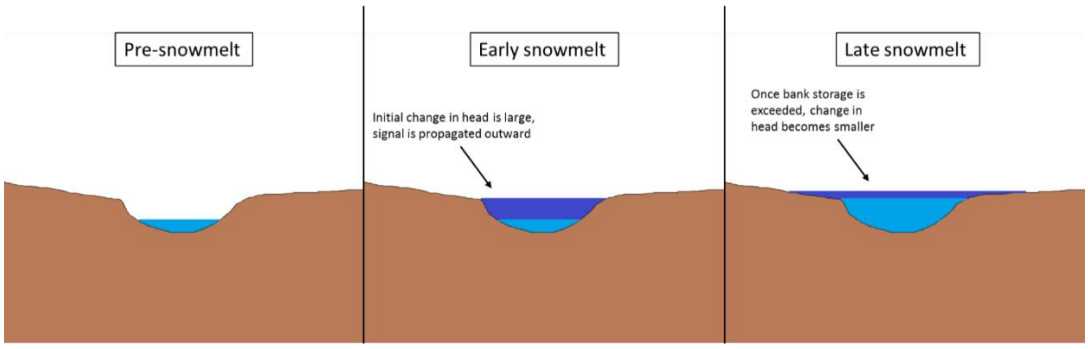

Figure 7.2: Diagram illustrating the reduced head change that occurs once bank storage in the swale is exceeded.

It is likely that this particular hillslope response to snowmelt includes components of both the depression-focused recharge model and the hillslope connectivity model. The depression-focused

recharge model describes the system response to rainfall well but the increased water input associated with snowmelt periods causes the hillslope connectivity model to circumvent it. This would explain why the hydraulic gradient reversed during both snowmelt seasons. Shifts in recharge mechanisms or flow directions during snowmelt periods are common in low-relief, till-dominated regions (Jones & Tomasek, 2015; Pam et al., 2020).

7.3) Fate of Snowmelt

Estimations of snowmelt infiltration using Equation 4.6 suggest that the majority of snowpack SWE (92%) did not infiltrate in the 2020 snowmelt season. Significant snowmelt delivery to surface waters likely began in late March, with $\delta^{18}O$ data suggesting that the swale and East Amity Creek responded six days following snowmelt onset (Figure 5.4b). This was corroborated by visual observations of water flowing over the land surface during this time. In 2021, the onset of snowmelt occurred in early March, which was multiple weeks earlier than 2020. Snowmelt delivery to the swale began one day after the onset of snowmelt, while shallow soil moisture response at the midslope and upslope sites began two days after the onset of snowmelt (Figure 5.10; Figure 5.12). The delayed response in the 15 cm sensors supports the notion that an ice lens at the base of the snowpack restricted snowmelt infiltration and water was thus routed via overland means. Snowmelt infiltration calculations suggested that roughly the same amount of snowmelt infiltrated in both study years, despite the first study year having a significantly higher snowpack SWE. This finding suggests that there may be a limit on the amount of infiltration that can occur in this system. This is consistent with the lack of soil moisture responses in the deeper soil sensors. It is possible that during periods of significant water input, such as snowmelt, the soil moisture storage capacity of the shallow soil is exceeded and further snowmelt infiltration is restricted.

Snowmelt surface runoff was difficult to quantify directly but could be inferred from piezometer, SWE, and stream stage data. The midslope piezometer response was larger in the 2021 snowmelt season relative to the 2020 snowmelt season despite a much lower amount of SWE in 2021. This finding indicates that a larger portion of snowpack SWE was lost to surface runoff during the 2020 snowmelt season. Additionally, stream stage in East Amity Creek reached similar peak values in both snowmelt seasons despite the lower amount of SWE in the 2021 snowmelt season (Figure 5.3d; Figure 5.11c). This suggests that a lower fraction of snowpack SWE was lost to surface runoff in the 2021 snowmelt season. However, at the location of the stream gauge, East Amity Creek drains an area of roughly 20 km^2, much larger than the area of the field site. Thus, stream stage data are more representative of surface runoff from the entire basin than from the field site itself.

Overall, piezometer, SWE, and stream stage data are in agreement that a larger amount of surface runoff occurred during the 2020 snowmelt season. Field studies in Sweden found similar patterns in runoff generation for years with differing amounts of snowpack; in years with smaller snowpacks, less snowmelt was partitioned into surface runoff (Nyberg et al., 2001; Stahli et al., 2001). Given that smaller snowpacks typically coincide with more extensive soil frost development, these findings corroborate the notion that soil frost alone is not a good indicator of surface runoff generation (Shanley & Chalmers, 1999; Nyberg et al., 2001). Rather, antecedent moisture conditions prior to snowmelt infiltration likely have a stronger influence on surface runoff generation. Considering the higher amount of rain during fall 2019, this corroborates other findings that wetter antecedent moisture conditions prior to snowmelt lead to enhanced runoff generation (Kane, 1980; Espeby, 1990; Shanley & Chalmers, 1999; Hardy et al., 2001; Pomeroy & Brun, 2001; Stahli et al., 2001).

7.4) Influence of Tile Drainage

The presence of legacy tile drainage at this particular site had implications for the hillslope response to precipitation and snowmelt. The main influence of the broken drain tile is the continuous input of water being discharged into the swale-hillslope system. The isotopic composition of the water discharged upstream of the swale resembled groundwater throughout most of the year except during snowmelt and very large (≥ 40 mm) rain events (Figure 5.4b). Due to the role of depressions in focusing recharge, the continuous input of water via broken drain tile has implications for shallow groundwater flow mechanisms in low-relief systems. For instance, the input of water from the discharge point to the hillslope depression leads to the development of a water table mound surrounding the swale. Normally, the formation of a water table mound is transient in nature and is an essential part of the depression-focused recharge mechanism (Johnsson & Lundin, 1991; Daniel & Staricka, 2000). However, the water table mound at this site may be quasi-permanent due to the constant input of water from the drain tile. Thus, shallow groundwater flow was away from the swale (from downslope to midslope, at depth) for the majority of the year except during snowmelt and post-melt periods (Figure 5.1d; Figure 5.2c; Figure 5.3c). This permanent water table mound maintains near-saturated conditions surrounding the swale, which would not allow for significant snowmelt or rainfall infiltration. Pam et al (2020) noted that the role of permanently ponded depressions may be less important than ephemerally ponded depressions in contributing to recharge. The tile drainage would likely decrease the role of depression-focused recharge in rainfall and snowmelt events, but the hillslope would be too dry for the hillslope connectivity model to control flow mechanisms throughout the year. As a result, the shift in recharge mechanisms would likely occur in the absence of the drain tile.

The constant input of water from the broken drain tile may also influence the development of soil frost. Under normal conditions, depressions are often dry at the end of the fall period and into the winter, allowing for the development of a soil frost layer underneath the

depression. The thawing of the frost layer during snowmelt then sets an upper limit on the rate of depression-focused recharge, and significant recharge does not occur until the frost layer has been sufficiently thawed (Baker & Spaans, 1997; Hayashi et al, 2003; Mohammed et al, 2019). This effect is highly localized to the depression itself and would likely not influence soil frost development surrounding the depression. Thus, a frozen layer can still form around the depression, which promotes runoff generation and accelerates depression-focused recharge. However, a constant input of relatively warm (7 - 9°C) water via broken drain tile would not allow for soil frost development underneath the depression at this particular field site. More in-depth studies on the role of artificial drainage networks on depression-focused recharge are needed to quantify the impact of soil frost on groundwater recharge in low-relief, glacial till-dominated systems.

7.5) Implications for Groundwater Recharge

The rapid and frequent response to precipitation in the piezometers across the two study years at the site suggests that shallow groundwater was recharged often throughout both the fall and spring. However, the responsiveness of the shallow (15 cm) soil moisture sensors coupled with the lack of response in the deeper (50 and 100 cm) sensors indicate that downward percolation of infiltrating water was limited. Thus, recharge via direct infiltration of meteoric waters was likely not a significant source of recharge to the piezometers. This corroborates findings from other studies of recharge in glacial till which note that recharge is dominated by the depression-focused mechanism (Fortin et al, 1991; Van Der Kamp & Hayashi, 1998; Jones & Tomasek, 2015; Pam et al, 2020).

The results of this study suggest a strong seasonal bias in groundwater recharge in northeastern Minnesota, which agrees with other recharge studies in the area (Delin et al., 2007; Dripps & Bradbury, 2007; Jones & Tomasek, 2015). The prominence of depression-focused recharge in formerly glaciated regions indicates that recharge is temporally limited to periods of

significant surface runoff generation, which can arise from limited infiltration (due to soil frost or near-saturated soils) and/or large amounts of water input. As a result, fall and spring represent important windows for recharge to occur in northeastern Minnesota (Delin et al., 2007). At my particular site, piezometer responses were largest during fall precipitation events and spring snowmelt events (Figure 5.1d; Figure 5.3c; Figure 5.11b). However, the midwinter rain event in December of 2019 also produced a significant piezometer response (Figure 5.2d). The lack of soil frost throughout the study made it difficult to assess the influence of frost dynamics on the timing of these recharge events. However, soil frost delays groundwater recharge primarily through inhibiting infiltration and percolation to the water table (Kane & Stein, 1983; Pomeroy & Brun, 2001; Stahli et al., 2001; Okkonen & Klove, 2011; Pittman et al., 2019). In formerly-glaciated regions, where direct groundwater recharge is scarce, soil frost may not have as strong of an influence on the timing and magnitude of recharge. In certain circumstances, soil frost may accelerate shallow recharge by routing a larger portion of snowmelt to topographical depressions. For example, the midslope piezometer responded to snowmelt one day sooner in 2021 when soil frost was present at the upslope site. In contrast, it is possible that soil frost could promote surface runoff generation to the extent that depression storage is exceeded and a fill-and-spill network is developed (Hayashi et al., 2003; Van der Kamp & Hayashi, 2009; Shaw et al., 2012). This network would route significant amounts of snowmelt away from the site, limiting the amount available for recharge.

A complicating factor in low-relief, till-dominated systems is that groundwater recharge may be somewhat ambiguous and hard to conceptually define. This ambiguity arises from the low permeability of the tills, which complicate the differentiation between the saturated and unsaturated zones (Lissey, 1971; Keller et al., 1988; Jones & Tomasek, 2015). In northeastern Minnesota, this ambiguity is further complicated by the presence of artificial drainage networks, which ultimately play a role in diverting shallow groundwater. Diverting water away from

depression will limit the role of depression-focused recharge and may cause a larger portion of water to be lost to evaporation (Keller et al., 1988; Hayashi & Van der Kamp, 2016). In low-permeability settings, surface water management practices such as irrigation or runoff diversion are thought to have a minimal effect on groundwater recharge since recharge is already limited in these settings (Keller et al., 1988). However, these systems can be highly active near the ground surface, and surface water management practices will undoubtedly influence these dynamics. The impact of artificial drainage networks on groundwater recharge processes should be examined in more detail.

The depression-focused recharge model explains the shallow groundwater dynamics of formerly glaciated systems under certain conditions. The model starts to break down under more complicated snowmelt scenarios and soil frost dynamics. The hillslope connectivity model presented by McNamara et al (2005) explains certain aspects of the field site's response to snowmelt, but its applicability to low-relief systems should be considered carefully. Additionally, the relevance of the depression-focused model for deeper groundwater recharge to intertill aquifers is unclear. Often, a shallow recharge pulse is entirely dissipated into the surrounding system before it can advance further downward (Keller et al, 1988; Hayashi et al, 2003). This lateral dissipation is likely what allows for rapid piezometer response following rain events. As a result, caution should be used when estimating recharge based on piezometer responses near depressions (Jones & Tomasek, 2015). Deeper groundwater recharge is likely very limited due to the extremely low hydraulic conductivity of the unweathered tills that exist at depth (Fortin et al, 1991; Hayashi et al, 2016).

Chapter 8: Conclusion

Sustainable groundwater management relies on an accurate understanding of groundwater recharge rates and mechanisms. In formerly-glaciated regions, the timing and quantification of groundwater recharge is complicated by low-permeability glacial tills and the presence of seasonally-frozen ground. In Northeastern Minnesota, remnant tile drainage further complicates groundwater recharge dynamics in current and abandoned agricultural systems. This study examined the relationship between precipitation, snowmelt, frost dynamics, and shallow groundwater processes through continuous monitoring of groundwater levels, soil water content, and soil temperature. Additionally, water sources and pathways throughout the system were identified using $\delta^{18}O$ and $\delta^{2}H$ from soil water, groundwater, precipitation, and streamflow. A conceptual model was developed to describe the system response to rainfall and snowmelt in order to understand better the groundwater processes active at the site. The conceptual model was also used to assess the role of tile drainage in altering shallow groundwater flow pathways.

My observations revealed a relatively dynamic shallow groundwater system in a low-relief, glacial-till agricultural field in Northeastern Minnesota. This dynamicity was due in part to a relatively permeable surficial soil layer and the influence of a century-old drain tile. The permeable surficial soil layer responded frequently to precipitation and snowmelt events, which contrasted the deeper soil layers that displayed an extremely limited response to precipitation and snowmelt. Thus, direct infiltration of meteoric waters was not a significant groundwater recharge mechanism. Rather, lateral subsurface flow and depression-focused recharge played a larger role in redistributing groundwater throughout the system. Recharge events were greatest during the fall and spring snowmelt periods. Despite the lack of groundwater response at deeper depths, soils at the site remained close to saturation throughout the duration of the study.

While the conceptual model described the system response to rainfall well, it began to break down during snowmelt periods. Primarily, the model could not describe a lack of snowmelt response at the downslope site. Stable isotope analysis revealed that lateral subsurface flow may play an important role in the system response to snowmelt and should be considered in the conceptual model. It is likely that multiple recharge mechanisms are active at the site throughout the year and that these mechanisms vary seasonally and spatially.

Quantifying the influence of tile drainage on the timing and magnitude of shallow recharge at the site proved difficult. Piezometer and soil moisture data at the downslope and midslope sites suggest that the main influence of the broken drain tile is the continuous input of water from the tile to the swale. In effect, persistent, drain-tile-sourced surface flow transformed the swale into a *losing* stream for most of the year. This input of water maintained artificially-high water levels within the swale, which limited the downslope piezometer response to snowmelt. Additionally, the water table mound formed from the continuous input of water maintained near-saturated conditions in deeper (50 – 100 cm depth) soil moisture sensors at the midslope site throughout most of the year. Tile-drainage influences were qualitative in nature and thus their quantitative impact on groundwater recharge at the site was unclear.

An overall lack of soil frost in both study years made it difficult to assess the influence of soil frost on the timing of groundwater recharge. However, there was an observed delay between the onset of snowmelt and the onset of soil moisture response. This delay was likely due to the presence of an ice lens at the base of the snowpack. Estimations of snowmelt partitioning revealed that both study years had roughly the same amount of snowmelt infiltration despite a much larger snowpack in the first study year. Surface runoff was notably higher in the first study year when soil water content was higher prior to snowmelt. Small amounts of soil frost at the upslope site in the second study year did not lead to increased runoff relative to the first study year, although the snowpack was much smaller in the second study year. The relationship

between frost dynamics, infiltration, and groundwater recharge is subject to change with a warming climate and thus more research into these relationships is needed. Smaller winter snowpacks, more frequent freeze/thaw cycles, and earlier snowmelts will all influence infiltration into frozen soils and, as a result, groundwater recharge. Frost dynamics, lateral flow, and tile drainage ultimately complicated the system response and thus more research is needed to assess how each of these components influence shallow groundwater processes.

References

Adomako, D., Maloszewski, P., Stumpp, C., Osae, S., Akiti, T. (2010). Estimating groundwater recharge from water isotope depth profiles in the Densu River basin, China. *Hydrological Sciences Journal*, 55(8), 1405-1416.

Baker, J., Spaans, E. (1997). Mechanisms of meltwater movement above and within frozen soil. *International Symposium on Physics, Chemistry, and Ecology of Seasonally Frozen Soils.*

Batelaan, O., Smedt, F. (2007). GIS-based recharge estimation by coupling surface subsurface water balances. *Journal of Hydrology*, 337(3-4), 337-355.

Benoit, G., Bornstein, J. (1970). Freezing and thawing effects on drainage. *Soil Science Society of America Journal*, 34(4), 551-557.

Berthold, S., Hayashi, M., Bentley, L. (2004). Integrated hydrogeological and geophysical study of depression-focused groundwater recharge in the Canadian prairies. *Water Resources Research*, 40(6).

Bevin, K., Germann, P. (1982). Macropores and water flow in soils. *Water Resources Research*, 18(5), 1311-1325.

Burt, T., Williams, P. (1976). Hydraulic conductivity in frozen soils. *Earth Surface Processes*, 1(4), 349-360.

Chesnaux, R. (2018). Avoiding confusion between pressure front pulse displacement and groundwater displacement: illustration with the pumping test in a confined aquifer. *Hydrological Processes*, 32(24), 3689-3694.

Chesnaux, R., Stumpp, C. (2018). Advantages and challenges of using soil water isotopes to assess groundwater recharge dominated by snowmelt at a field study located in Canada. *Hydrological Sciences Journal*, 63(5).

Chifflard, P., Blume, T., Maerker, K., Hopp, L., van Meerveld, I., Graef, T., Gronz, O., Hartmann, A., Kohl, B., Martini, E., Reinhardt-Imjela, C., Reiss, M., Rinderer, M., Achleitner, S. (2018). How can we model subsurface stormflow at the catchment scale if we cannot measure it? *Hydrological Processes*, 33(9), 1378-1385.

Clark, I., Fritz, P. (1997). Environmental Isotopes in Hydrogeology. CRC Press.

Craig, H. (1961). Isotopic variations in meteoric waters. *Science*, 133(3465), 1702-1703.

Cuthbert, M., Mackay, R., Tellam, J., Thatcher, K. (2010). Combining unsaturated and saturated hydraulic observations to understand and estimate groundwater recharge through glacial till. *Journal of Hydrology*, 391(3-4), 263-276.

Daniel, J., Staricka, J. (2000). Frozen soil impact on groundwater-surface water interaction. *Journal of the American Water Resources Association*, 36(1), 151-160.

D'Astous, A., Ruland, W., Bruce, J., Cherry, J., Gillham, R. (1989). Fracture effects in the shallow groundwater zone in weathered Sarnia-area clay. *Canadian Geotechnical Journal*, 26(1).

Delin, G., Healy, R., Lorenz, D., Nimmo, J. (2007). Comparison of local- to regional-scale estimate of groundwater recharge in Minnesota, USA. *Journal of Hydrology*, 334(1-2), 231-249.

Desaulniers, D., Cherry, J., Fritz, P. (1981). Origin, age, and movement of pore water in argillaceous Quaternary deposits at four sites in southwestern Ontario. *Journal of Hydrology*, 50, 231-257.

Dripps, W., Bradbury, K. (2007). A simply daily soil-water balance model for estimating the spatial and temporal distribution of groundwater recharge in temperate humid areas. *Hydrogeology Journal*, 15, 433-444.

Dripps, W., Bradbury, K. (2009). The spatial and temporal variability of groundwater recharge in a forested basin in northern Wisconsin. *Hydrological Processes*, 24(4), 383-392.

Duk-Rodkin, A., Hughes, O. (1994). Tertiary-quaternary drainage of the pre-glacial Mackenzie basin. *Quaternary International*, 22-23, 221-241.

Earman, S., Campbell, A., Phillips, F., Newman, B. (2006). Isotopic exchange between snow and atmospheric water vapor: estimation of the snowmelt component of groundwater recharge in the southwestern United States. *Journal of Geophysical Research: Atmospheres*, 111(D9).

Espeby, B. (1990). Tracing the origin of natural waters in a glacial till slope during snowmelt. *Journal of Hydrology*, 118(1-4), 107-127.

Fortin, G., van der Kamp, G., Cherry, J. (1991). Hydrogeology and hydrochemistry of an aquifer-aquitard system within glacial deposits, Saskatchewan, Canada. *Journal of Hydrology*, 126(3-4), 265-292.

Fritz, P., Cherry, J., Sklash, M, Weyer, K. (1976). Storm runoff analysis using environmental isotopes and major ions. *International Atomic Energy Agency (IAEA)*: IAEA.

Gerber, R., Boyce, J., Howard, K. (2001). Evaluation of heterogeneity and field-scale groundwater flow regime in a leaky till aquitard. Hydrogeology Journal, 9, 60-78.

Granger, R., Gray, D., Dyck, G. (1984). Snowmelt infiltration to frozen prairie soils. *Canadian Journal of Earth Sciences*, 21(6), 669-677.

Gray, D., Landine, P., Granger, R. (1985). Simulating infiltration into frozen prairie soils in streamflow models. *Canadian Journal of Earth Sciences*, 22(3).

Gucker, C. (2009). Tanacetum vulgare. Fire Effects Information System, U.S. Department of Agriculture, Forest Service, Rocky Mountain Research Station, Fire Sciences Laboratory.

Hardy, J., Groffman, P., Fitzhugh, R., Henry, K., Welman, A., Demers, J., Fahey, T., Driscoll, C., Tierney, G., Nolan, S. (2001). Snow depth manipulation and its influence on soil frost and water dynamics in a northern hardwood forest. *Biogeochemistry*, 56, 151-174.

Hayashi, M., van der Kamp, G., Schmidt, R. (2003). Focused infiltration of snowmelt water in partially frozen soil under small depressions. *Journal of Hydrology*, 270(3-4), 214-229.

Hayashi, M., van der Kamp, G., Rosenberry, D. (2016). Hydrology of prairie wetlands: understanding the integrated surface-water and groundwater processes. *Wetlands*, 36(2), 237-254.

Heath, R. (1983). Basic ground-water hydrology. *Water Supply Paper 2220,* United States Geological Survey.

Heinze, T., Blöcher, J. (2019). A model of local thermal non-equilibrium during infiltration. *Advances in Water Resources*, 132.

Hendry, M. (1988). Hydrogeology of clay till in a prairie region of Canada. *Groundwater*, 26(5), 607-614.

Hendry, M., Kelln, C., Wassenaar, L., Shaw, J. (2004). Characterizing the hydrogeology of a complex clay-rich aquitard system using detailed vertical profiles of the stable isotopes of water. *Journal of Hydrology*, 293(1-4), 47-56.

Henry, H. (2008). Climate change and soil freezing dynamics: historical trends and projected changes. *Climatic Change*, 87, 421-434.

Iwata, Y., Nemoto, M., Hasegawa, S., Yanai, Y., Kuwao, K., Hirota, T. (2011). Influence of rain, air temperature, and snow cover on subsequent spring-snowmelt infiltration into thin frozen soil layer in northern Japan. *Journal of Hydrology*, 401(3-4), 165-176.

Jansson, P., Gustafson, A. (1987). Simulation of surface runoff and pipe discharge from an agricultural soil in Northern Sweden. *Hydrology Research*, 18(3), 151-166.

Johnsson, H., Lundin, L. (1991). *Surface runoff and soil water percolation as affected by snow and soil frost*. Journal of Hydrology, 122(1-4), 141-159.

Jones, P., Tomasek, A. (2015). Assessment of aquifer properties, evapotranspiration, and the effects of ditching in the Stoney Brook watershed, Fond du Lac Reservation, Minnesota, 2006-9. *U.S. Geological Survey Scientific Investigations Report 2015-5007*.

Kane, D. (1980). Snowmelt infiltration into seasonally frozen soils. *Cold Regions Science and Technology*, 3(2-3), 153-161.

Kane, D., Stein, J. (1983). *Water movement into seasonally frozen soils*. Water Resources Research, 19(6).

Keller, C., van der Kamp, G., Cherry, J. (1988). Hydrogeology of two Saskatchewan tills, I. Fractures, bulk permeability, and spatial variability of downward flow. *Journal of Hydrology*, 101(1-4), 97-121.

Kim, S. (2009). Characterization of soil moisture responses on a hillslope to sequential rainfall events during late autumn and spring. *Water Resources Research*, 45(9).

Lee, K., Kim, Y. (2007). Determining the seasonality of groundwater recharge using water isotopes: a case study from the Upper North Han River basin, Korea. *Environmental Geology*, 52, 853-859.

Lissey, A. (1971). Depression-focused transient groundwater flow patterns in Manitoba. *Geological Association of Canada Special Papers*, 9, 333-341.

Lundberg, A., Ala-Aho, P., Eklo, O., Klöve, B., Kværner, J., Stumpp, C. (2015). Snow and frost: implications for spatiotemporal infiltration patterns – a review. *Hydrological Processes*, 30(8).

McConville, C., Kalin, R., Johnston, H., McNeill, G. (2005). Evaluation of recharge in a small temperate catchment using natural and applied $\delta^{18}O$ profiles in the unsaturated zone. *Groundwater*, 39(4).

McNamara, J., Chandler, D., Seyfried, M., Achet, S. (2005). Soil moisture states, lateral flow, and streamflow generation in a semi-arid, snowmelt-driven catchment. Hydrological Processes, 19, 4023-4038.

Minnesota Groundwater Association (2018). Drain tiles and groundwater resources: understanding the relations. *Minnesota Groundwater Association White Paper 03*.

Mohammed, A., Kurylyk, B., Cey, E., Hayashi, M. (2018). Snowmelt infiltration and macropore flow in frozen soils: overview, knowledge gaps, and a conceptual framework. *Vadose Zone Journal*, 17(1): 1-15.

Mohammed, A., Pavlovskii, I., Cey, E., Hayashi, M. (2019). Effects of preferential flow on snowmelt partitioning and groundwater recharge in frozen soils. Hydrology and Earth Systems Sciences, 23(12), 5017-5031.

Mueller, M., Alaoui, A., Kuells, C., Leistert, H., Meusburger, K., Stumpp, C., Weiler, M, Alewell, C. (2014). Tracking water pathways in steep hillslopes by $\delta^{18}O$ depth profiles of soil water. *Journal of Hydrology*, 519, 340-352.

Nolan, B., Baehr, A., Kauffman, L. (2003). Spatial variability of groundwater recharge and its effect on shallow groundwater quality in southern New Jersey. *Vadose Zone Journal*, 2(4), 677-691.

Nyberg, L., Stähli, M., Mellander, P., Bishop, K. (2001). Soil frost effects on soil water and runoff dynamics along a boreal forest transect: 1. Field investigations. *Hydrological Processes*, 15(4).

O'Driscoll, M., DeWalle, D., McGuire, K., Gburek, W. (2005). Seasonal ^{18}O variations and groundwater recharge for three landscape types in central Pennsylvania, USA. *Journal of Hydrology*, 303(1-4), 108-124.

Okkonen, J., Jyrkama, M., Kløve, B. (2009). A conceptual approach for assessing the impact of climate change on groundwater and related surface waters in cold regions (Finland). *Hydrogeology Journal*, 18, 429-439.

Okkonen, J., Kløve, B. (2011). A sequential modelling approach to assess groundwater surface water resources in a snow dominated region of Finland. *Journal of Hydrology*, 411(1-2), 91-107.

Pam, E., Ireson, A., van der Kamp, G., Hendry, J. (2020). Ephemeral ponds: are they the dominant source of depression-focused recharge? *Water Resources Research*, 56(3).

Pavlovskii, I., Hayashi, M., Lennon, M. (2018). Transformation of snow isotopic signature along groundwater recharge pathways in the Canadian Prairies. *Journal of Hydrology*, 563, 1147-1160

Pavlovskii, I., Hayashi, M., Itenfisu, D. (2019). Midwinter melts in the Canadian Prairies: energy balance and hydrological effects. *Hydrology and Earth System Science*, 23(4).

Pawluk, S. (1988). Freeze-thaw effects on granular structure reorganization for soil materials of varying texture and moisture content. Canadian Journal of Soil Science, 68(3).

Pittman, F., Mohammed, A., Cey, E. (2019). *Effects of antecedent moisture and macroporosity on infiltration and water flow in frozen soil.* Hydrological Processes, 34(3).

Pomeroy, J., Brun, E. (2001). Physical properties of snow. *Cambridge University Press: Cambridge*; 45-126.

Ruland, W., Cheery, J., Feenstra, S. (1991). The depth of fractures and active groundwater flow in a clayey till plan in Southwestern Ontario. Groundwater, 29(3), 405-417.

Saxena, R., Dressie, Z. (1984). Estimation of groundwater recharge and moisture movement in sandy formations by tracing natural oxygen-18 and injected tritium profiles in the unsaturated zone. *International Atomic Energy Agency (IAEA)*: IAEA.

Shanley, J., Chalmers, A. (1999). The effect of frozen soil on snowmelt runoff at Sleepers River, Vermont. *Hydrological Processes*, 13(12-13).

Sharratt, B. (2001). Groundwater recharge during spring thaw in the Prairie Pothole Region via large, unfrozen preferential pathways. *American Society of Agricultural and Biological Engineers*, St. Joseph, Michigan.

Shaw, D., Van der Kamp, G., Conly, M., Pietroniro, A., Martz, L. (2011). The fill-spill hydrology of prairie wetland complexes during drought and deluge. *Hydrological Processes*, 26(20), 3147-3156.

Smith, E., Westenbroek, S. (2015). Potential groundwater recharge for the State of Minnesota using the soil-water balance model, 1996-2010. *U.S. Geological Survey Scientific Investigations Report, 2015-5038.*

Stähli, M., Nyberg, L., Mellander, P., Jansson, P., Bishop, K. (2001). Soil frost effects on soil water and runoff dynamics along a boreal transect: 2. Simulations. *Hydrological Processes*, 2001, 15(6).

Stumpp, C., Hendry, J. (2012). Spatial and temporal dynamics of water flow and solute transport in a heterogenous glacial till: the application of high-resolution profiles of $\delta^{18}O$ and $\delta^{2}H$ in pore waters. *Journal of Hydrology*, 438-439, 203-214.

Thorne, G., Laporte, J., Clarke, D. (1998). The effects of frozen soils on groundwater recharge and discharge in granitic rock terrane of the Canadian Shield. *Nordic Hydrology*, 29(4-5), 371-384.

Thunholm, B., Lundin L., Lindell, S. (1989). Infiltration into a Frozen Heavy Clay Soil. *Nordic Hydrology*, 20, 153-166.

Trost, J., Maher, A., Simpkins, W., Witt, A., Stark, J., Blum, J., Berg, A. (2020). Hydrogeology and groundwater geochemistry of till confining units and confined aquifers in glacial deposits near Litchfield, Cromwell, Akeley, and Olivia, Minnesota, 2014-18. *U.S. Geological Survey Scientific Investigations Report 2020*-5127, 80.

Van der Kamp, G., Hayashi, M. (1998). The groundwater recharge function of small wetlands in the semi-arid northern prairies. *Great Plains Research*, 8(1), 39-56.

Van der Kamp, G., Hayashi, M. (2003). Comparing the hydrology of grassed and cultivated catchments in the semi-arid Canadian prairies. *Hydrological Processes*, 17(3), 559-575.

Van der Kamp, G., Hayashi, G. (2009). Groundwater-wetland ecosystem interaction in the semiarid glaciated plans of North America. *Hydrogeology Journal*, 17, 203-214.

de Vries, J., Simmers, I. (2002). Groundwater recharge: an overview of processes and challenges. *Hydrogeology Journal*, 10, 5-17.

Watanabe, K., Kito, T., Wu, J., Greer, C., Flury, M. (2012). Water infiltration into a frozen soil with simultaneous melting of the frozen layer. Vadose Zone Journal, 12(1).

Watanabe, K., Kugisaki, Y. (2017). Effect of macropores on soil freezing and thawing with infiltration. Hydrological Processes, 31(2), 270-278.

Weigert, A., Schmidt, J. (2005). Water transport under winter conditions. *Catena*, 64(2-3), 193-208.

Weiler, M., McDonnell, J., Tromp-van Meerveld, I., Uchida, T. (2006). Subsurface stormflow. *Encyclopedia of Hydrological Sciences*, 112.

Winograd, I., Riggs, A., Coplen, T. (1998). The relative contributions of summer and cool-season precipitation to groundwater recharge, Spring Mountains, Nevada, USA. *Hydrogeology Journal*, 6, 77-93.

Zernitz, E. (1932). Drainage patterns and their significance. *Journal of Geology*, 40(6), 498-521.

Zhang, M., Zhang, X., Lu, J., Pei, W., Wang, C. (2018). Analysis of volumetric unfrozen water contents in freezing soils. *Experimental Heat Transfer*, 32(5): 426-438.

Zhao, L., Gray, D. (1997). A parametric expression for estimating infiltration into frozen soils. *Hydrological Processes*, 11(13), 1761-1775.

Zhao, L., Gray, D. (1999). Estimating snowmelt infiltration into frozen soils. *Hydrological Processes*, 13(12-13).

Appendix 1: Particle Size Analysis Results and Estimation of Saturation

Table A1: Particle Size Analysis for the upslope, midslope, and downslope sites based on methods presented by Gee & Bauder (1986).

Site	Horizon	Depth Range (cm)	% Sand	% Clay	% Silt	Soil Texture
Upslope	A	0 – 10	59.03	9.55	31.42	Sandy Loam
Upslope	A/B	10 – 25	52.57	10.69	36.74	Sandy Loam
Upslope	B	25 – 42	52.89	9.09	38.02	Sandy Loam
Upslope	B/C	42 – 66	41.38	15.19	43.43	Loam
Midslope	A	0 – 20	55.73	9.82	34.45	Sandy Loam
Midslope	A/B	20 – 35	42.04	11.15	46.81	Loam
Midslope	B	35 – 50	47.41	12.15	40.44	Loam
Midslope	B/C	50 – 60	33.42	20.40	46.18	Loam
Midslope	C1	60 – 73	31.34	16.31	52.35	Silt Loam
Midslope	C2	73 – 95	46.64	14.24	39.12	Loam
Downslope	A	0 – 30	53.45	10.16	36.38	Sandy Loam
Downslope	A/B	30 – 61	54.09	9.14	36.77	Sandy Loam
Downslope	B	61 – 70	47.97	13.59	38.43	Loam
Downslope	B/C	71 – 85	41.44	16.32	42.24	Loam
Downslope	C	85 – 98	28.69	18.43	52.87	Silt Loam

Table A2: Estimations of field saturation for each sensor depth at each site based on methods presented by Chandler et al., 2017.

Site	15 cm depth	50 cm depth	100 cm depth
Upslope	0.537 cm^3/cm^3	0.464 cm^3/cm^3	0.375 cm^3/cm^3
Midslope	0.495 cm^3/cm^3	0.550 cm^3/cm^3	0.504 cm^3/cm^3

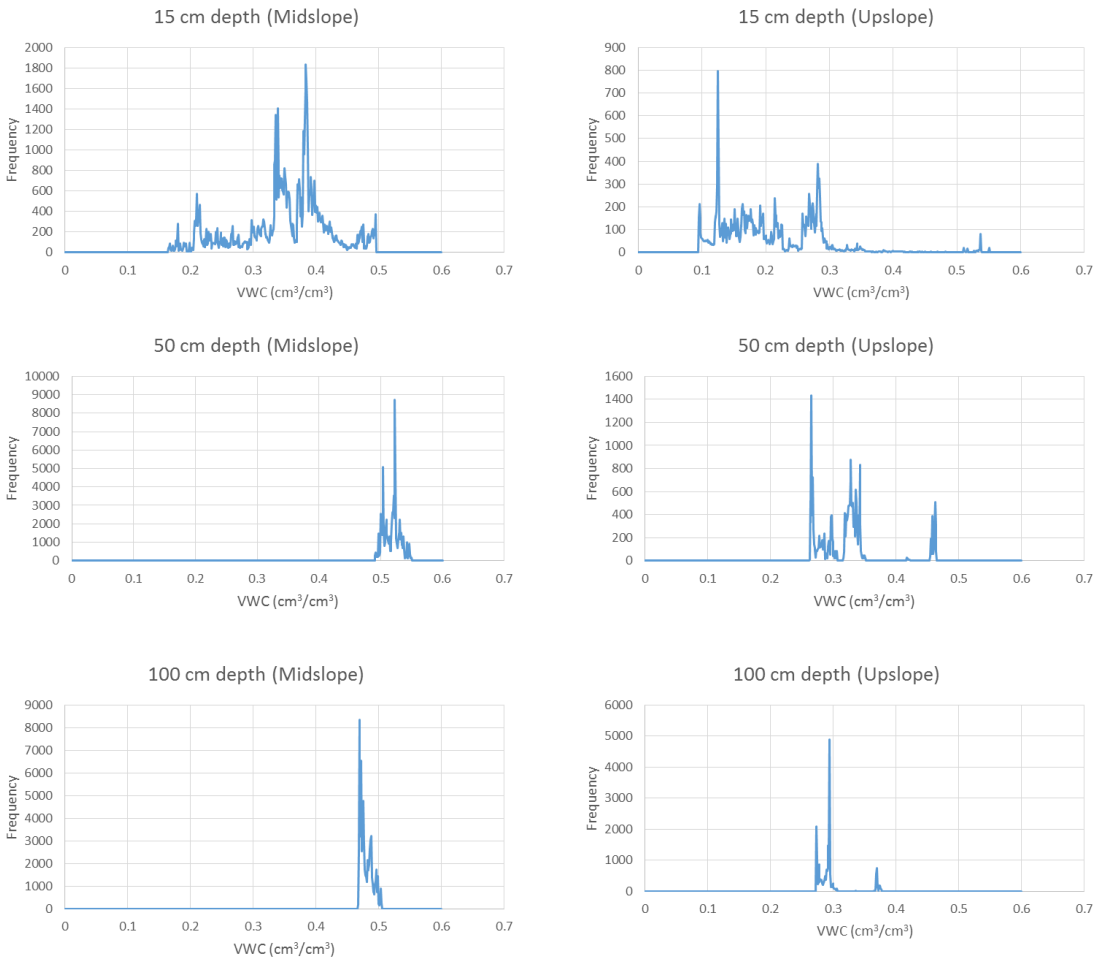

Figure A1: Frequency analyses used to estimate field saturation for each depth at each site.

Appendix 2: East Amity Creek Profile Data

Procedure:

Stream discharge was calculated by discretizing the channel into trapezoids of uniform width (20 cm). Depth measurements were taken at each 20 cm interval and thus an area in cm^2 could be calculated using the formula:

$$A = \left(\frac{Depth_1 + Depth_2}{2}\right) * 20$$

Velocity measurements in m/s were taken at each 20 cm interval using a 2100LX Flow Meter from Swoffer. Area was converted to m^2 and multiplied by velocity to calculate discharge through each "trapezoid". Discharges from every trapezoid were summed to calculate the total discharge through the stream channel.

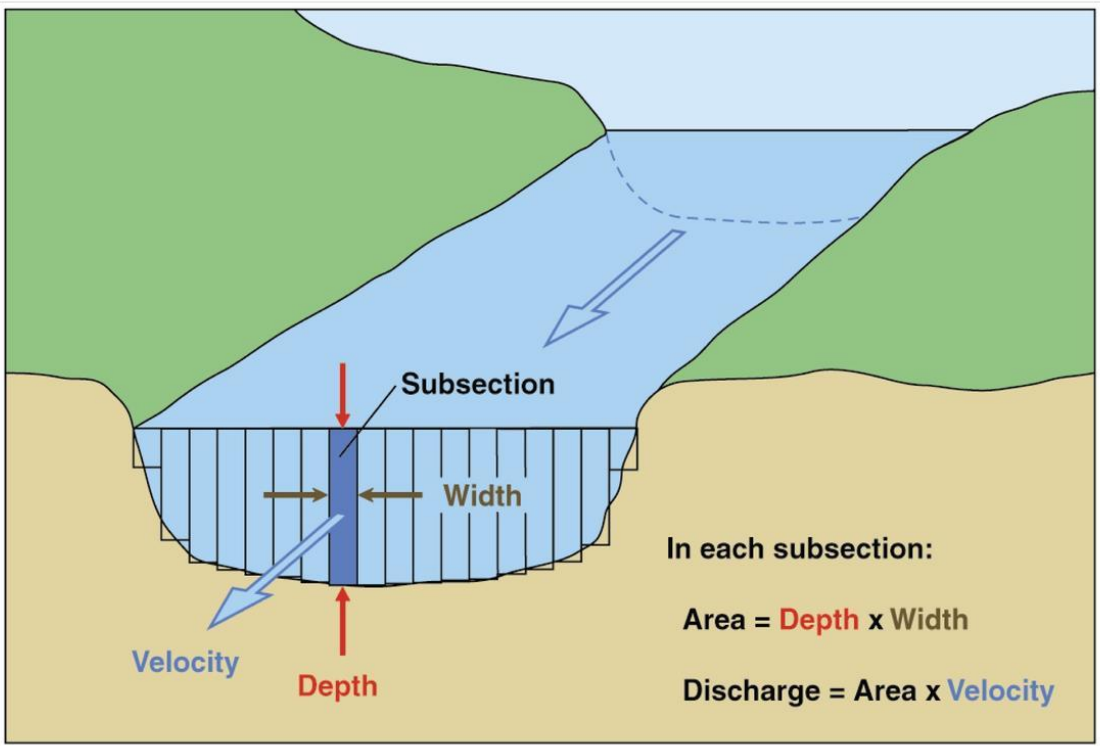

Table A2: Stage and discharge measurements from the East Branch of Amity Creek, 2019 – 2021.

Date	Stage (m)	Discharge (m^3/s)
7/10/2019	0.281	0.036
8/29/2019	0.252	0.01
9/10/2019	0.401	0.296
5/22/2020	0.302	0.061
6/11/2020	0.285	0.009
7/10/2020	0.366	0.156
8/10/2020	0.322	0.065
9/4/2020	0.25	0.005
10/15/2020	0.355	0.052
11/15/2020	0.325	0.104
3/30/2021	0.528	0.655